SIAM J. NUMER. ANAL.
Vol. 59, No. 5, pp. 2536–2570

FAST MULTISCALE GAUSSIAN BEAM METHOD FOR THREE-DIMENSIONAL ELASTIC WAVE EQUATIONS IN BOUNDED DOMAINS*

JIANLIANG QIAN† AND CHAO SONG‡

Abstract. We propose a new fast multiscale Gaussian beam method to solve the three-dimensional elastic wave equation in a bounded domain in the high-frequency regime. We develop a novel multiscale transform to decompose an arbitrary vector-valued function into multiple Gaussian wavepackets with various resolutions. We consider both periodic and Dirichlet boundary conditions, and we further derive various reflection rules to compute crucial multiscale Gaussian beam ingredients so as to enforce these boundary conditions. To improve efficiency and accuracy of multiscale beam propagation, we develop a new reinitialization strategy based on the stationary phase approximation so that we can sharpen each single beam. Such a reinitialization strategy is especially useful and necessary to treat the shear-wave reflection. Numerical examples in different setups demonstrate correctness and robustness of the new method. We also show numerically that the convergence rate of the proposed multiscale Gaussian beam method follows that of the classical Gaussian beam solution, i.e., $O(\frac{1}{\sqrt{\omega}})$, where ω is the largest frequency in the underlying wave motion.

Key words. multiscale Gaussian wavepacket transform, multiscale Gaussian beam, elastic waves, eikonal equations

AMS subject classifications. 65N30, 65M60

DOI. 10.1137/20M1386116

1. Introduction.

The elastic wave equation is essential for modeling wave propagation and solving wave-related inverse problems in seismology [1]. Different from the scalar acoustic wave motion, multiple wave modes simultaneously propagate in the vectorial elastic wave motion. We propose a novel multiscale Gaussian beam method to solve the elastic wave equation with different boundary conditions at high frequencies in inhomogeneous media.

To mitigate dispersion errors due to high frequencies in numerical wave propagation, popular direct methods, such as finite-difference or finite-element methods, require extremely refined meshes. Therefore, some alternative methods have been developed, such as geometrical optics (GO). Applying the usual GO ansatz to wave equations yields an asymptotic solution in terms of a real-valued phase function and a real-valued amplitude function; however, the amplitude function blows up at caustics, where the phase function becomes multivalued, so that the usual GO ansatz fails at caustics.

To resolve caustics, the Gaussian beam method as an extension of the GO ansatz for wave equations relaxes the restriction that the phase function is real-valued. A single Gaussian beam solution is defined in terms of quantities on a central ray so that an elementary beam solution consists of a phase function and an amplitude function,

*Received by the editors December 14, 2020; accepted for publication (in revised form) June 28, 2021; published electronically October 4, 2021.
https://doi.org/10.1137/20M1386116
Funding: The work of the authors was partially supported by the National Science Foundation.
†Departments of Mathematics and CMSE, Michigan State University, East Lansing, MI 48824 USA (qian@math.msu.edu, http://www.math.msu.edu/~qian/).
‡Department of Mathematics, Michigan State University, East Lansing, MI 48824 USA (songchao@math.msu.edu).

both of which are globally defined, complex-valued, and approximate. Away from the central ray path, the single beam solution decays rapidly like a Gaussian profile. A superposition of many such single beams yields an asymptotically correct solution of the underlying wave equation so that both the wave equation and the initial-boundary conditions are satisfied in the high-frequency regime.

To apply the Gaussian beam method to solve wave equations, the first problem is how to initialize beams in terms of generic initial conditions. Since Gaussian beams essentially serve as a solution operator (wave propagator) to wave equations, we ask the following question: can we link Gaussian beams to the recent works on the optimal representation of the wave propagator? In fact, several frames, such as the curvelet [26, 10, 9] and the wave atom [12, 13], both of which follow the so-called parabolic scaling principle, have been developed to optimally represent a wave propagator. We say that a wavepacket satisfies the parabolic scaling principle if the wavelength of the typical oscillation of this wavepacket is equal to the square of the width of this wavepacket.

Motivated by these optimal representations, the multiscale Gaussian wavepacket transform was developed in [24] for scalar wave equations. Since the Hamiltonian of the underlying scalar wave equation is homogeneous of degree one, which essentially constrains the resulting Hamiltonian flow to the cosphere bundle, a Gaussian beam satisfies the parabolic scaling principle throughout its evolution. In this paper, we extend this idea further to treat vector-valued initial conditions for elastic wave equations so as to preserve advantages of the multiscale Gaussian wavepacket transform; based on this vectorized multiscale transform, we further develop a fast multiscale Gaussian beam method for elastic wave equations.

To apply the Gaussian beam method to solve initial-boundary value problems of wave equations, the second problem is to derive reflection dynamics for wave propagation in a bounded domain. Most recently in the paper [4], a novel method has been proposed for the acoustic wave equation. Other discussions about Gaussian beam reflections for scalar wave equations can be found in [7, 25]. However, it is more complicated to treat beam reflections for elastic wave equations since two different wave modes propagate simultaneously in the system. Consequently, beam reflections in the elastic wave case need to deal with conversion of wave modes, where the mode conversion is unique for the elastic wave equation.

To carry out long-term beam propagation for the elastic wave equation, the third problem is how to reinitialize beam propagation efficiently. Although the beam ansatz is capable of treating caustics, Gaussian beams will lose accuracy in long-term wave propagation in some situations. As analyzed in [23, 24], the width of a beam may grow exponentially during the evolution process; this implies that the beam loses its localized significance, leading to deteriorating accuracy in the Taylor expansion for the phase function and high cost in the beam summation. Therefore, various methods have been developed to control the width of a single beam. One possible approach, the so-called beam-reinitialization method, is to apply the multiscale Gaussian wavepacket transform to decompose a superposed Gaussian beam solution into Gaussian wavepackets, and the resulting Gaussian wavepackets enable us to restart the beam propagation [24, 4]. In this paper, we propose a new beam-reinitialization method, which is more flexible and yields an asymptotic solution to the elastic wave equation. Instead of dealing with the superposed wavefield, the new strategy treats each single beam individually so that we are able to develop a more efficient reinitialization method by using special structures of beam components and the parabolic scaling principle.

To summarize, our new multiscale Gaussian beam method for elastic wave equations enjoys several advantages. First of all, the beam ansatz resolves caustics

automatically. Second, a novel multiscale Gaussian wavepacket transform is developed to decompose generic vector-valued initial conditions. Similar to its scalar version, the multiscale Gaussian wavepacket transform defines an optimal set of frames to characterize the elastic wave propagator. Third, a stationary phase approximation based reinitialization procedure is developed to improve the beam accuracy in long-term wave propagation.

1.1. Related work. The existence of Gaussian beam solutions for wave equations has been known to the pure mathematics community since sometime in the 1960s [2], and these solutions have been used to obtain results on propagation of singularities in hyperbolic PDEs [25, 15]. A crucial point of beam dynamics is to have a global solution to the Ricatti equation defining the Hessian of the phase function so that a beam solution has a well-localized Gaussian profile globally [25, 22, 28]; consequently, an essential point for Gaussian beams to prevail is that possible caustics can be treated automatically, since there is a high probability for so-called transmission caustics to occur in inhomogeneous media [29].

Gaussian beam methods are applicable to many problems, for example, seismic wave modeling, quantum mechanics, and underwater acoustics [11, 14, 23]. An Eulerian Gaussian beam method for the Helmholtz wave equation was proposed in [20], and the Eulerian method was further developed for semiclassical quantum mechanics in [18, 19].

The fact that the Hamiltonian of the underlying wave equation is homogeneous of degree one guarantees the parabolic scaling principle to hold at any given time, which provides the theoretical basis for our new reinitialization method as the size of a multiscale Gaussian wavepacket can be analyzed. It has been stated in [8, 26] that a wavepacket will remain a wavepacket at a later time if it satisfies the parabolic scaling principle and the Hamiltonian is smooth. There are various types of such wavepackets, such as curvelets [10, 9] and wave atoms [12]. Our new multiscale Gaussian wavepacket transform is appropriately modified to adapt to Gaussian beam dynamics in elastic wave motion.

1.2. Contents. The rest of the paper is organized as follows. In section 2, we develop Gaussian beam methods for elastic wave equations. In section 3, we extend the multiscale Gaussian wavepacket transform [24] to the vector-valued initial conditions of elastic wave equations and develop new propagation dynamics for each single Gaussian beam. After proposing the decomposition scheme, we discuss how to implement multiscale beams for periodic boundary value problems in section 4 and we further derive reflection dynamics for the homogeneous Dirichlet boundary condition in section 5. We carry out stationary phase analysis of beams in section 6. The differences among various types of reflections are analyzed in section 7 and a new efficient reinitialization method is proposed to resolve those differences in section 7.3. In section 8, numerical experiments are conducted to demonstrate the performance of our new algorithm.

2. Asymptotic methods for elastic wave equations. We consider the following initial-boundary value problem of the elastic wave equation:

$$0 = \rho\ddot{\boldsymbol{u}} - \nabla\lambda(\nabla\cdot\boldsymbol{u}) - \nabla\mu\cdot(\nabla\boldsymbol{u} + \nabla\boldsymbol{u}^T) - (\lambda+\mu)\nabla(\nabla\cdot\boldsymbol{u}) - \mu\Delta\boldsymbol{u}, \tag{2.1}$$

where $\boldsymbol{u}$ is the displacement vector, ρ is the density parameter, the parameters λ and μ are known as the Lame parameters, and

$$\dot{\boldsymbol{u}} = \frac{\partial \boldsymbol{u}}{\partial t}; \quad \ddot{\boldsymbol{u}} = \frac{\partial^2 \boldsymbol{u}}{\partial t^2}. \tag{2.2}$$

The Lame parameters are assumed to be smooth, positive, and bounded away from zero. The initial conditions are specified as follows:

$$\boldsymbol{u}(\boldsymbol{x}, 0) = \boldsymbol{f}(\boldsymbol{x}); \quad \boldsymbol{u}_t(\boldsymbol{x}, 0) = \boldsymbol{g}(\boldsymbol{x}), \tag{2.3}$$

where the functions $\boldsymbol{f}$ and $\boldsymbol{g}$ are compactly supported vector-valued functions in the space $[L_2(R^d)]^d$. In the following presentation, we take $\rho = 1$ without loss of generality.

We are looking for asymptotic solutions for the elastic wave equation (2.1) with two different types of boundary conditions: the periodic boundary condition and the homogeneous Dirichlet boundary condition,

$$\boldsymbol{u}(\boldsymbol{x}, t)\Big|_{\partial\Omega\times[0,T]} = \mathbf{0}. \tag{2.4}$$

2.1. Some notation. To simplify derivations, we introduce some notation.

- $\dot{\tau} = \frac{\partial \tau}{\partial t}$.
- $|\cdot|$ denotes the Euclidean norm in $\mathbb{R}^d$.
- $\mathbf{v}^T$ denotes the transpose of vector $\mathbf{v}$.
- $\nabla = (\frac{\partial}{\partial x_1}, \ldots, \frac{\partial}{\partial x_d})^T$.
- $\cdot$ represents the inner product between two column vectors.
- $\tau_{,k} = \partial\tau/\partial x_k$.

In addition, the Einstein summation convention will be assumed.

2.2. Eikonal equations for P- and S-waves. Applying the GO ansatz to the elastic wave equation and considering the leading-order singularity [17, 1], we end up with the following equation for elastic waves:

$$(\lambda + \mu)\nabla\tau\nabla\tau^T \boldsymbol{A} = (\dot{\tau}^2 - \mu\tau_{,k}\tau_{,k})\boldsymbol{A}, \tag{2.5}$$

where τ and $\boldsymbol{A}$ are unknown phase and amplitude functions, respectively. The equation having nontrivial solutions leads to an eigenvalue problem, resulting in two different wave modes, the P- and the S-wave, with appropriately chosen phases and amplitudes.

When the amplitude vector $\boldsymbol{A} = \boldsymbol{A}^P$ is parallel to $\nabla\tau$, we have the P-wave eikonal equation,

$$(\dot{\tau}^P)^2 - (\lambda + 2\mu)(\tau^P_{,k}\tau^P_{,k}) = 0, \tag{2.6}$$

where we denote τ^P and $\boldsymbol{A}^P$ the P-wave eikonal and the amplitude vector, respectively.

When the amplitude vector $\boldsymbol{A} = \boldsymbol{A}^S$ is orthogonal to $\nabla\tau$, we have the S-wave eikonal equation,

$$(\dot{\tau}^S)^2 - \mu(\tau^S_{,k}\tau^S_{,k}) = 0, \tag{2.7}$$

where we denote τ^S and $\boldsymbol{A}^S$ the S-wave eikonal and the amplitude vector, respectively.

To compute τ^P and τ^S, we can apply the method of characteristics to the nonlinear eikonal equations (2.6) and (2.7). Since these two eikonal equations are essentially the same, we consider them generically as a Hamilton–Jacobi equation in the following form:

$$\dot{\tau}^{P,S} + G^{P,S}(\boldsymbol{x}, \nabla\tau) = 0, \tag{2.8}$$

where the Hamiltonian of the P-wave is $G^P(\boldsymbol{x},\boldsymbol{p}) = \pm\sqrt{\lambda+2\mu}|\boldsymbol{p}|$ and the Hamiltonian of the S-wave is $G^S(\boldsymbol{x},\boldsymbol{p}) = \pm\sqrt{\mu}|\boldsymbol{p}|$. We consider the P-wave case as an illustration so that the method of characteristics yields

$$\begin{cases} \frac{d\boldsymbol{x}}{dt} = G^P_{\boldsymbol{p}}(\boldsymbol{x}(t),\boldsymbol{p}(t)), \quad \boldsymbol{x}(0) = \boldsymbol{x}_0; \\ \frac{d\boldsymbol{p}}{dt} = -G^P_{\boldsymbol{x}}(\boldsymbol{x}(t),\boldsymbol{p}(t)), \quad \boldsymbol{p}(0) = \boldsymbol{p}_0, \end{cases} \tag{2.9}$$

where t is the running parameter of a bicharacteristic.

Solving this Hamiltonian system yields a bicharacteristic in phase space

$$\{(\boldsymbol{x}(t),\boldsymbol{p}(t)) : t \geq 0\},$$

where the associated ray is $\gamma = \{\boldsymbol{x}(t) : t \geq 0\}$, the $\boldsymbol{x}$-component of a bicharacteristic. Moreover, we have $\boldsymbol{p}(t) = \nabla\tau(t,\boldsymbol{x}(t))$ along the ray γ due to the method of characteristics.

One of the most significant differences between the Gaussian beam method and other ray-theory methods is that the phase function of a Gaussian beam is complex-valued. To be more specific, the second-order derivative (the Hessian) of the phase function is designed to be complex-valued. To derive the dynamics of the Hessian matrix, we first differentiate the eikonal equation (2.8) with respect to t and $\boldsymbol{x}$ near the ray γ,

$$\dot{\tau}^P_{\boldsymbol{x}} + G^P_{\boldsymbol{x}} + \tau^P_{\boldsymbol{xx}} G^P_{\boldsymbol{p}} = 0, \tag{2.10}$$

$$\ddot{\tau}^P + (G^P_{\boldsymbol{p}})^T \dot{\tau}^P_{\boldsymbol{x}} = 0. \tag{2.11}$$

Differentiating (2.10) with respect to $\boldsymbol{x}$ again yields

$$\dot{\tau}^P_{\boldsymbol{xx}} + G^P_{\boldsymbol{xx}} + \tau^P_{\boldsymbol{xx}} G^P_{\boldsymbol{xp}} + (G^P_{\boldsymbol{xp}})^T \tau^P_{\boldsymbol{xx}} + \tau^P_{\boldsymbol{xx}} G^P_{\boldsymbol{pp}} \tau^P_{\boldsymbol{xx}} + \tau^P_{\boldsymbol{xxx}} G^P_{\boldsymbol{p}} = 0. \tag{2.12}$$

Since (2.11), (2.10), and (2.12) are valid along the ray, the Hessian $M^P(t) = \tau^P_{\boldsymbol{xx}}$ of the phase function along the ray satisfies the following Ricatti equation:

$$\frac{dM^P}{dt} + G^P_{\boldsymbol{xx}} + M^P G^P_{\boldsymbol{xp}} + (G^P_{\boldsymbol{xp}})^T M^P + M^P G^P_{\boldsymbol{pp}} M^P = 0. \tag{2.13}$$

The same derivation can be applied to the S-wave with $G^S(\boldsymbol{x},\boldsymbol{p}) = \pm\sqrt{\mu}|\boldsymbol{p}|$. One essential property of the Gaussian beam solution is that it will remain well-localized throughout propagation if it is so initially, and this localization property is made possible by enforcing the imaginary part of the Hessian M to be symmetric positive definite (SPD). The following lemma [25] guarantees this property throughout the propagation for all smooth ray trajectories.

LEMMA 2.1. *If the Hamiltonian G is smooth enough, then the Hessian $M(t)$ along the ray path γ has an SPD imaginary part, provided that it initially does.*

Accordingly, the Hessian of the phase function of a beam solution is well-defined even at caustics.

2.3. Transport equation for P-wave amplitude vector. Since the amplitude vector $\boldsymbol{A}^P$ for the P-wave is parallel to the ray direction $\nabla\tau^P$, the P-wave

amplitude can be written as $\boldsymbol{A} = a\nabla\tau^P$, where a is a scalar function. To avoid cluttered notation, we write τ^P as τ in this subsection. After some calculations [17, 1], we have the transport equation for the scalar function a,

$$\dot{a} + \frac{(\lambda+2\mu)a_{,k}\tau_{,k}}{G} + \frac{a}{2G}\left((\lambda+2\mu)\text{trace(M)} - \ddot{\tau}\right) = 0. \tag{2.14}$$

Although the second-order derivatives of the phase function τ appear in the transport equation (2.14), the P-wave transport equation has a well-defined solution since Lemma 2.1 guarantees a well-defined Hessian of the phase function along a ray.

Following [24], the transport equation for a can be added to the P-wave dynamics by using (2.14) and $\frac{d\boldsymbol{x}}{dt} = G_{\boldsymbol{p}}$,

$$\frac{da(t,\boldsymbol{x}(t))}{dt} + \frac{a}{2G}((\lambda+2\mu)\text{trace}(M) - G_{\boldsymbol{x}}\cdot G_{\boldsymbol{p}} - G_{\boldsymbol{p}}^T M G_{\boldsymbol{p}}) = 0. \tag{2.15}$$

2.4. Transport equation for S-wave amplitude vector. We abbreviate τ^S as τ in this subsection. We first write the amplitude vector as $\boldsymbol{A}^S = \tilde{a}\boldsymbol{D}$, where $\tilde{a}$ is a scalar function, and $\boldsymbol{D}$ is a unit vector which is orthogonal to the ray direction $\nabla\tau^S$.

We find that the scalar function $\tilde{a}$ satisfies

$$2\dot{\tilde{a}}\dot{\tau} + \tilde{a}\ddot{\tau} = \mu(2\tau_{,k}\tilde{a}_{,k} + \tilde{a}\tau_{,kk}), \tag{2.16}$$

which takes the same form as the P-wave transport equation. Therefore, we can obtain the same ODE as the P-wave case (2.15).

Unlike the P-wave, we need one more equation to describe the direction $\boldsymbol{D}$ of the amplitude vector $\boldsymbol{A}^S$. Since the direction $\boldsymbol{D}$ is orthogonal to $\boldsymbol{p}(t) = (p_k(t)) = \nabla\tau(t,\boldsymbol{x}(t))$, we have

$$\begin{aligned} 0 &= \frac{d(D_k p_k)}{dt}, \\ 0 &= \frac{dD_k}{dt}p_k + \frac{dp_k(t)}{dt}D_k, \\ \frac{dD_k}{dt} &= -\left(\frac{dp_j(t)}{dt}D_j\right)\frac{p_k(t)}{|p(t)|^2}, \end{aligned} \tag{2.17}$$

where we have used the property that $\boldsymbol{D}$ is a unit vector so that $\frac{d\boldsymbol{D}}{dt}$ is parallel to $\boldsymbol{p}(t)$.

2.5. Single beam solutions for P- and S-waves. To summarize the ODE dynamics generated by the method of characteristics, we have

$$\begin{aligned} \frac{d\boldsymbol{x}}{dt} &= G_{\boldsymbol{p}}(\boldsymbol{x}(t),\boldsymbol{p}(t)), \quad \boldsymbol{x}(0) = \boldsymbol{x}_0, \\ \frac{d\boldsymbol{p}}{dt} &= -G_{\boldsymbol{x}}(\boldsymbol{x}(t),\boldsymbol{p}(t)), \quad \boldsymbol{p}(0) = \boldsymbol{p}_0, \\ \frac{dM}{dt} &= -(G_{\boldsymbol{xp}})^T M - MG_{\boldsymbol{px}} - MG_{\boldsymbol{pp}}M - G_{\boldsymbol{xx}}, \quad M(0) = i\epsilon I, \\ \frac{da}{dt} &= -\frac{a}{2G}\left(c^2\text{trace}(M) - G_{\boldsymbol{x}}\cdot G_{\boldsymbol{p}} - G_{\boldsymbol{p}}^T M G_{\boldsymbol{p}}\right), \quad A(0) = A_0, \end{aligned} \tag{2.18}$$

where the velocity term $c^2 = \lambda + 2\mu$ for the P-wave and $c^2 = \mu$ for the S-wave, and G is the corresponding Hamiltonian, respectively.

There is one extra equation for the direction $\boldsymbol{D}$ in the S-wave dynamics from (2.17),

$$\frac{d\boldsymbol{D}}{dt} = -\left(\frac{d\boldsymbol{p}}{dt}\cdot\boldsymbol{D}\right)\frac{\boldsymbol{p}(t)}{|\boldsymbol{p}(t)|^2}, \quad \boldsymbol{D}(0)=\boldsymbol{D}_0. \tag{2.19}$$

The initial condition of the above system will be specified according to the multiscale Gaussian wavepacket transform, which will be presented in section 3. Once the phase functions $\tau^{P,S}$ and the amplitude vectors $\boldsymbol{A}^{P,S}$ are available, we can construct a single-beam asymptotic solution in the following way:

$$\Phi^P(t,\boldsymbol{x}) = a^P(t)\nabla\tau^P(t,\boldsymbol{x}(t))e^{i\omega\tau^P(t,\boldsymbol{x})}, \tag{2.20}$$

$$\Phi^S(t,\boldsymbol{x}) = a^S(t)\boldsymbol{D}^S e^{i\omega\tau^S(t,\boldsymbol{x})}, \tag{2.21}$$

where the phase function is approximated by the Taylor expansion near the central ray,

$$\begin{aligned}\tau^{P,S}(t,\boldsymbol{x}) &= \nabla\tau^{P,S}\cdot(\boldsymbol{x}-\boldsymbol{x}^{P,S}(t)) + \frac{1}{2}(\boldsymbol{x}-\boldsymbol{x}^{P,S}(t))^T M^{P,S}(t)(\boldsymbol{x}-\boldsymbol{x}^{P,S}(t))\\ &= \boldsymbol{p}^{P,S}(t)\cdot(\boldsymbol{x}-\boldsymbol{x}^{P,S}(t)) + \frac{1}{2}(\boldsymbol{x}-\boldsymbol{x}^{P,S}(t))^T M^{P,S}(t)(\boldsymbol{x}-\boldsymbol{x}^{P,S}(t)).\end{aligned} \tag{2.22}$$

The desired Gaussian profile is induced by the imaginary part of the Hessian matrix $M^{P,S}$,

$$\exp\left(-\frac{\omega}{2}(\boldsymbol{x}-\boldsymbol{x}^{P,S}(t))^T\mathrm{Im}(M^{P,S}(t))(\boldsymbol{x}-\boldsymbol{x}^{P,S}(t))\right). \tag{2.23}$$

As suggested by Lemma 2.1, a beam solution will always be well-localized throughout propagation.

3. Multiscale wavepacket transform for elastic waves. Since the initial conditions of the elastic wave equation (2.3) can be any general L_2 vector-valued functions, they may not take the form of Gaussian wavepackets,

$$\boldsymbol{A}\exp\left(i\omega\left(\boldsymbol{p}(0)^T(\boldsymbol{x}-\boldsymbol{x}_0)+\frac{1}{2}(\boldsymbol{x}-\boldsymbol{x}_0)^T M(0)(\boldsymbol{x}-\boldsymbol{x}_0)\right)\right). \tag{3.1}$$

The problem here is how to decompose any general L_2 function into multiple Gaussian wavepackets in the above form (3.1) efficiently and make the total number of computed beams as small as possible.

In this section we will first provide a brief introduction to the multiscale Gaussian wavepacket transform [24] for scalar functions. Afterward, we will extend the construction of the scalar case to that of the vectorial case.

3.1. Multiscale Gaussian wavepacket transforms: Scalar case. We first partition the Fourier or frequency space $\mathbb{R}^d$ into several Cartesian coronae C_l for $l \geq 1$ as

$$C_l = \left\{\boldsymbol{\xi} = (\xi_1,\xi_2,\ldots,\xi_d) : \max_{1\leq i\leq d}|\xi_i| \in [4^{l-1},4^l]\right\}.$$

Now it is obvious to see that the size of $\boldsymbol{\xi}$ in C_l is of $O(4^l)$. For each C_l, we further partition it into multiple windows with width 2^l,

$$B_{l,i} = \prod_{s=1}^{d}[2^l i_s, 2^l(i_s+1)],$$

where the integer multi-index $(i_1, i_2, \ldots, i_d)$ is any possible choice such that the box is in the lth layer, i.e., $B_{l,i} \subset C_l$. After defining these cell boxes $B_{l,i}$, we define the Gaussian profile $g_{l,i}$ associated with the box $B_{l,i}$ by the following formula:

$$g_{l,i}(\boldsymbol{\xi}) \approx e^{-\left(\frac{|\boldsymbol{\xi}-\boldsymbol{\xi}_{l,i}|}{\sigma_l}\right)^2}, \tag{3.2}$$

where $\boldsymbol{\xi}_{l,i}$ is the center of the box $B_{l,i}$ and $\sigma_l = 2^{l-1}$ is the width of the box $B_{l,i}$.

To have a partition of unity, we also define conjugate filters $h_{l,i}$ such that

$$h_{l,i}(\boldsymbol{\xi}) = \frac{g_{l,i}(\boldsymbol{\xi})}{\sum_{l,i}(g_{l,i}(\boldsymbol{\xi}))^2}. \tag{3.3}$$

The proof that the functions $h_{l,i}$ are well-defined and well-localized can be found in [24]. It is easy to see that $\sum_{l,i} g_{l,i} h_{l,i} = 1$. Moreover, we define Gaussian wavepackets in the frequency domain by using

$$\hat{\phi}_{l,i,k}(\boldsymbol{\xi}) = \frac{1}{L_l^{d/2}} e^{-2\pi i \frac{k\boldsymbol{\xi}}{L_l}} g_{l,i}(\boldsymbol{\xi}),$$
$$\hat{\psi}_{l,i,k}(\boldsymbol{\xi}) = \frac{1}{L_l^{d/2}} e^{-2\pi i \frac{k\boldsymbol{\xi}}{L_l}} h_{l,i}(\boldsymbol{\xi}).$$

Taking the inverse Fourier transforms yields their definitions in the spatial domain,

$$\phi_{l,i,k}(\boldsymbol{x}) = \frac{1}{L_l^{d/2}} \int_{R^d} e^{2\pi i(\boldsymbol{x}-\frac{k}{L_l})\cdot\boldsymbol{\xi}} g_{l,i}(\boldsymbol{\xi}) d\boldsymbol{\xi}, \tag{3.4}$$

$$\psi_{l,i,k}(\boldsymbol{x}) = \frac{1}{L_l^{d/2}} \int_{R^d} e^{2\pi i(\boldsymbol{x}-\frac{k}{L_l})\cdot\boldsymbol{\xi}} h_{l,i}(\boldsymbol{\xi}) d\boldsymbol{\xi}. \tag{3.5}$$

We cite a useful lemma from [24] without proof.

LEMMA 3.1. *For any $f \in L_2(\mathbb{R}^d)$, we have*

$$f(\boldsymbol{x}) = \sum_{l,i,k} \langle \psi_{l,i,k}, f \rangle \phi_{l,i,k}(\boldsymbol{x}). \tag{3.6}$$

Since the idea of decomposing discrete signals into multiple wavepackets is very similar to the continuous case, we skip this part and provide the pseudocode below.

Algorithm 3.1. Discrete multiscale Gaussian wavepacket decomposition

1. Apply the fast Fourier transform to the discrete signal f.
2. Compute $h_{l,i}(\boldsymbol{\xi})\hat{f}(\boldsymbol{\xi})$.
3. Wrap the result to the domain $[-2\sigma_l, 2\sigma_l]$.
4. Apply the inverse Fourier transform to obtain coefficients $c_{l,i,k}$.

The computational complexity of this algorithm is $O\left(N^d \log N\right)$, where N is the number of sampling points in each direction.

3.2. Multiscale Gaussian wavepacket transform: Vectorial case. Having at our disposal the multiscale Gaussian wavepacket transform for scalar functions, we are ready to extend this transform to the vector-valued function $\boldsymbol{f}$, where we assume that each component f_j of the vector $\boldsymbol{f}$ is an L_2 function.

3.2.1. Decomposition of a single Gaussian wavepacket. Suppose we have already applied the multiscale Gaussian wavepacket transform to each component of the initial condition $\boldsymbol{f}$, i.e.,

$$\boldsymbol{f} = (f_1, f_2, \ldots, f_d)^T = \sum_{l,i,k} \boldsymbol{\kappa}_{l,i,k}\phi_{l,i,k},$$

where the superscript T denotes transpose. The purpose here is to decompose each single Gaussian wavepacket into a sum of P- and S-wave components.

Let the unit vector $\boldsymbol{v}_{l,i,k}$ be $\frac{\boldsymbol{\xi}_{l,i}}{|\boldsymbol{\xi}_{l,i}|}$. Then we can decompose $\boldsymbol{\kappa}_{l,i,k}$ into two components,

$$\boldsymbol{\kappa}_{l,i,k} = \left(\boldsymbol{\kappa}_{l,i,k}^T \boldsymbol{v}_{l,i,k}\right) \boldsymbol{v}_{l,i,k} + \left(I_d - \boldsymbol{v}_{l,i,k}(\boldsymbol{v}_{l,i,k})^T\right) \boldsymbol{\kappa}_{l,i,k}. \tag{3.7}$$

The first term on the right-hand side of (3.7) is taken to be the P-wave component, and the initial condition for its amplitude vector can be written as

$$\left(\boldsymbol{\kappa}_{l,i,k}^T \boldsymbol{v}_{l,i,k}\right) \boldsymbol{v}_{l,i,k} = \left(\boldsymbol{\kappa}_{l,i,k}^T \frac{\boldsymbol{\xi}_{l,i}}{|\boldsymbol{\xi}_{l,i}|^2}\right) \boldsymbol{\xi}_{l,i}. \tag{3.8}$$

To initialize the S-wave component, we have to specify initial directions which are orthogonal to each other and at the same time are orthogonal to $\boldsymbol{v}_{l,i,k}$. Therefore, we choose the first direction $\boldsymbol{D}^{(1)}$ as the unit vector of the first column vector of the matrix $(I_d - \boldsymbol{v}_{l,i,k}(\boldsymbol{v}_{l,i,k})^T)$ and apply the Gram–Schmidt process to generate the other columns $\boldsymbol{D}^{(m)}$ for $m = 2, \ldots, d-1$. Since every column vector of the matrix $(I_d - \boldsymbol{v}_{l,i,k}(\boldsymbol{v}_{l,i,k})^T)$ is orthogonal to $\boldsymbol{v}_{l,i,k}$, their linear combinations are orthogonal to $\boldsymbol{v}_{l,i,k}$ as well. The corresponding amplitude coefficients a_m are

$$a_m = \boldsymbol{\kappa}_{l,i,k}^T \left(I_d - \boldsymbol{v}_{l,i,k}(\boldsymbol{v}_{l,i,k})^T\right) \boldsymbol{D}^{(m)}, \quad m = 1, 2, \ldots, d-1. \tag{3.9}$$

3.2.2. Preprocessing initial conditions for wavepacket transform. Before applying the method described above, we preprocess the initial conditions first. Following the same strategy employed in [24], we consider two different branches, $\boldsymbol{\kappa}_{l,i,k}^+$ and $\boldsymbol{\kappa}_{l,i,k}^-$, for each wavepacket corresponding to different signs of the Hamiltonian $\pm c(\boldsymbol{x})|\boldsymbol{p}|$, where $c(\boldsymbol{x})$ is the corresponding velocity of the P- and the S-wave, respectively.

To satisfy both the initial displacement $\boldsymbol{f}$ and the initial velocity $\boldsymbol{g}$, we define

$$(\boldsymbol{\kappa}_{l,i,k}^+ + \boldsymbol{\kappa}_{l,i,k}^-)\phi_{l,i,k} = \boldsymbol{\kappa}_{l,i,k}\phi_{l,i,k} = \boldsymbol{f}. \tag{3.10}$$

Taking the derivative of the wavefield with respect to time t yields

$$\left(\boldsymbol{\kappa}_{l,i,k}^- - \boldsymbol{\kappa}_{l,i,k}^+\right) \left(i|\boldsymbol{\xi}_{l,i}|G^+(\boldsymbol{x}_0, \boldsymbol{p}_0)\right) \phi_{l,i,k} \approx \boldsymbol{\Xi}_{l,i,k}\phi_{l,i,k} = \boldsymbol{g}, \tag{3.11}$$

where $\boldsymbol{\Xi}_{l,i,k}$ are the coefficients generated from decomposing the initial velocity $\boldsymbol{g}$. Here the left-hand side of (3.11) is not the complete form of the beam's time derivative; instead, we keep only the leading-order term to approximate this derivative in the asymptotic sense.

After solving for coefficients $\boldsymbol{\kappa}_{l,i,k}^+$ and $\boldsymbol{\kappa}_{l,i,k}^-$ from (3.10) and (3.11), we can apply the decomposition described in (3.7) and (3.9) to $\boldsymbol{\kappa}_{l,i,k}^+$ and $\boldsymbol{\kappa}_{l,i,k}^-$, respectively.

We summarize the vector-valued multiscale Gaussian wavepacket transform into the following algorithm.

Algorithm 3.2. Discrete wavepacket transform of vector-valued initial conditions $\boldsymbol{f}$ and $\boldsymbol{g}$

1. Apply the discrete Gaussian wavepacket transform to each component in the discrete signals $\boldsymbol{f}$ and $\boldsymbol{g}$.
2. Use (3.10) and (3.11) to compute $\boldsymbol{\kappa}^{+}_{l,i,k}$ and $\boldsymbol{\kappa}^{-}_{l,i,k}$.
3. Generate the P-wave amplitude vector $\left(\boldsymbol{\kappa}^{\pm}_{l,i,k}\cdot\frac{\boldsymbol{\xi}_{l,i}}{|\boldsymbol{\xi}_{l,i}|^2}\right)\boldsymbol{\xi}_{l,i}$.
4. Generate the S-wave amplitude vector $a_m\boldsymbol{D}^{(m)}$ by (3.9) for $m=1,2,\ldots,d-1$.

While the above process defines the initial amplitude vectors for the P- and S-waves, the initial values of the P- and S-wave phase functions and their related derivatives are specified according to the multiscale Gaussian wavepacket transform of the scalar form. Therefore, we have the following beam dynamics for the P- and the S-wave, respectively:

$$\begin{aligned}
\frac{d\boldsymbol{x}}{dt} &= G_{\boldsymbol{p}}(\boldsymbol{x}(t),\boldsymbol{p}(t)), \quad \boldsymbol{x}(0)=\frac{\boldsymbol{k}}{L_l},\\
\frac{d\boldsymbol{p}}{dt} &= -G_{\boldsymbol{x}}(\boldsymbol{x}(t),\boldsymbol{p}(t)), \quad \boldsymbol{p}(0)=2\pi\frac{\boldsymbol{\xi}_{l,i}}{|\boldsymbol{\xi}_{l,i}|},\\
\frac{dM}{dt} &= -(G_{\boldsymbol{xp}})^T M - MG_{\boldsymbol{px}} - MG_{\boldsymbol{pp}}M - G_{\boldsymbol{xx}}, \quad M(0)=i(2\pi^2\sigma_l^2/|\boldsymbol{\xi}_{l,i}|)I,\\
\frac{da}{dt} &= -\frac{a}{2G}\left(c^2\mathrm{trace}(M) - G_{\boldsymbol{x}}\cdot G_{\boldsymbol{p}} - G_{\boldsymbol{p}}^T M G_{\boldsymbol{p}}\right), \quad a(0)=\left(\sqrt{\frac{\pi}{L_l N}}\sigma_l\right)^d,\\
\frac{d\boldsymbol{D}^{(m)}}{dt} &= -\left(\frac{d\boldsymbol{p}}{dt}\cdot\boldsymbol{D}^{(m)}\right)\frac{\boldsymbol{p}}{|\boldsymbol{p}|^2}, \quad \boldsymbol{D}^{(m)}(0)=\boldsymbol{D}^{(m)}.
\end{aligned}$$

Once asymptotic ingredients are available, the P-wave solution takes the form

$$\Phi^p(t,\boldsymbol{x}) = a(t,\boldsymbol{x}(t))\boldsymbol{p}(t)e^{i|\boldsymbol{\xi}_{l,i}|\tau^P(t,\boldsymbol{x})}, \tag{3.12}$$

where τ^P is given in the formula (2.22). In the following computation, however, we absorb the large wavenumber $|\boldsymbol{\xi}_{l,i}|$ into the phase function by modifying the corresponding initial conditions of beam dynamics, and the resulting solution is equivalent to the explicit one as shown in the following.

Denote the beam using the usual initial condition as $(\boldsymbol{x}_t,\boldsymbol{p}_t,M_t,a_t,\boldsymbol{D}_t)$ and that using the initial condition $(\boldsymbol{x}_0,|\boldsymbol{\xi}_{l,i}|\boldsymbol{p}_0,|\boldsymbol{\xi}_{l,i}|M_0,a_0,\boldsymbol{D}_0)$ as $(\hat{\boldsymbol{x}}_t,\hat{\boldsymbol{p}}_t,\hat{M}_t,\hat{a}_t,\hat{\boldsymbol{D}}_t)$. Using ray theory, we have

$$\begin{aligned}
\frac{d\boldsymbol{x}_t}{dt} &= c(\boldsymbol{x}_t)\frac{|\boldsymbol{\xi}_{l,i}|\boldsymbol{p}_t}{|\boldsymbol{\xi}_{l,i}||\boldsymbol{p}_t|}, \quad \boldsymbol{x}_0=\frac{\boldsymbol{k}}{L_l},\\
\frac{d(|\boldsymbol{\xi}_{l,i}|\boldsymbol{p}_t)}{dt} &= \nabla c(\boldsymbol{x}_t)|\boldsymbol{\xi}_{l,i}||\boldsymbol{p}_t|, \quad |\boldsymbol{\xi}_{l,i}|\boldsymbol{p}_0=2\pi\boldsymbol{\xi}_{l,i}.
\end{aligned}$$

It is obvious that $(\boldsymbol{x}_t,|\boldsymbol{\xi}_{l,i}|\boldsymbol{p}_t)$ is the solution of the Hamiltonian system with the same initial condition as $(\hat{\boldsymbol{x}}_t,\hat{\boldsymbol{p}}_t)$. Therefore, by the uniqueness of solution for the initial value problem, $\hat{\boldsymbol{p}}_t=|\boldsymbol{\xi}_{l,i}|\boldsymbol{p}_t$ and $\hat{\boldsymbol{x}}_t=\boldsymbol{x}_t$.

We multiply $|\boldsymbol{\xi}_{l,i}|$ on both sides of the Ricatti equation,

$$\begin{aligned}\frac{d(|\boldsymbol{\xi}_{l,i}|M)}{dt} &= -\nabla\nabla c(\boldsymbol{x}_t)|\boldsymbol{\xi}_{l,i}||\boldsymbol{p}_t| - |\boldsymbol{\xi}_{l,i}|M\nabla c\frac{|\boldsymbol{\xi}_{l,i}|\boldsymbol{p}_t}{|\boldsymbol{\xi}_{l,i}||\boldsymbol{p}_t|} - |\boldsymbol{\xi}_{l,i}|\nabla c\left(\frac{|\boldsymbol{\xi}_{l,i}|\boldsymbol{p}_t}{|\boldsymbol{\xi}_{l,i}||\boldsymbol{p}_t|}\right)^T M \\ &\quad - (|\boldsymbol{\xi}_{l,i}|M)\left(\frac{c(\boldsymbol{x}_t)}{|\boldsymbol{\xi}_{l,i}||\boldsymbol{p}_t|}I - \frac{c(\boldsymbol{x}_t)}{|\boldsymbol{\xi}_{l,i}||\boldsymbol{p}_t|^3}\boldsymbol{p}_t\boldsymbol{p}_t^T\right)(|\boldsymbol{\xi}_{l,i}|M) \\ &= -\nabla\nabla c(\hat{\boldsymbol{x}}_t)|\hat{\boldsymbol{p}}_t| - \hat{M}G_{\boldsymbol{xp}}(\hat{\boldsymbol{x}}_t,\hat{\boldsymbol{p}}_t) - G_{\boldsymbol{xp}}^T(\hat{\boldsymbol{x}}_t,\hat{\boldsymbol{p}}_t)\hat{M} - \hat{M}G_{\boldsymbol{pp}}(\hat{\boldsymbol{x}}_t,\hat{\boldsymbol{p}}_t)\hat{M}.\end{aligned}$$

By the uniqueness of solution for the initial value problem, $\hat{M}_t = |\boldsymbol{\xi}_{l,i}|M_t$. Similar computations can be carried out for the magnitude and direction of amplitude vectors.

4. Multiscale beams for periodic boundary value problems. To solve the periodic boundary value problem, all ingredients are assumed to be periodic functions. Meanwhile, the central ray in the periodic boundary value problem is smooth during propagation in the periodic sense.

The principle shown in Figure 1 will be employed to solve the periodic boundary value problem, where the cubic region $[0, 0.5]^3$ is chosen to test the correctness of our algorithm. The red dashed line represents the wavepacket leaving the domain $[0, 0.5]$, as the left half goes beyond the domain and the right half is still inside the domain. The missing left half of the beam solution will enter from the other side with the same shape, which is the blue line in the graph suggested by the periodic boundary condition. We show numerical results in section 8.

5. Multiscale Gaussian beams for homogeneous Dirichlet boundary conditions. In this section, we design multiscale Gaussian beams to satisfy homogeneous Dirichlet boundary conditions. Since the three-dimensional (3-D) elastic wave motion shows much more interesting features than the 2-D case, we will work out the details for elastic waves in the 3-D space $\{\boldsymbol{x} = (x, y, z) : x, y, z \in \mathbb{R}\}$.

The time-dependent wavefield on the boundary vanishes since the homogeneous Dirichlet boundary condition is imposed. When a ray hits the boundary at time t^r and location $\boldsymbol{x}(t^r)$ and subsequently reflects into the domain, the sum of all wave modes at time t^r and the central point $\boldsymbol{x}(t^r)$ vanishes, i.e., $\boldsymbol{u}(t^r, \boldsymbol{x}(t^r)) = 0$. The time when the central point $\boldsymbol{x}(t^r)$ of the ray is on the boundary is defined as the reflection time, and the central point as the reflection point.

Tacitly, all equations in this section are defined on the point $(t^r, \boldsymbol{x}(t^r))$, if not specified. The Hamiltonian used in this section is assumed to be positive, $G = c(\boldsymbol{x})|\boldsymbol{p}|$, and the negative Hamiltonian will be treated similarly.

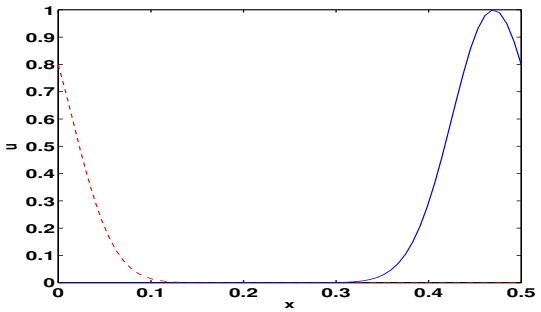

FIG. 1. *Periodic boundary condition with a wavepacket leaving the boundary.*

5.1. P-wave reflecting beams: Ray directions. When a P-wave reflection happens, the total wavefield consists of three different sources, the original P-wave Gaussian beam, a new P-wave beam after reflection, namely, the P-to-P or PP beam, and a new S-wave beam after reflection, namely, the P-to-S or PS beam. At the reflection point $\boldsymbol{x}(t^r)$, we have

$$-a^P e^{i\tau^P}\nabla\tau^P = a^{PP}e^{i\tau^{PP}}\nabla\tau^{PP} + a^{PS}e^{i\tau^{PS}}\boldsymbol{D}^{PS}, \tag{5.1}$$

since both P- and S-waves will be generated after reflection.

All phase functions should have the same value at the reflection point, $\tau^P = \tau^{PP} = \tau^{PS}$; otherwise, if we change the value of the large wavenumber $|\boldsymbol{\xi}_{l,i}|$, the homogeneous boundary condition will be violated.

We derive new phase functions τ^{PP} and τ^{PS} using the continuity condition, namely, the continuity of the tangential components of the first-order derivatives of τ, so that we have

$$\tau_y^P = \tau_y^{PP} = \tau_y^{PS} \quad \text{and} \quad \tau_z^P = \tau_z^{PP} = \tau_z^{PS}, \tag{5.2}$$

where we assume that the reflection happens along the surface $\{\boldsymbol{x} = (x, y, z) : x = 0\}$. Moreover, the partial derivative of the phase function with respect to time t also satisfies the continuity condition,

$$\dot{\tau}^P = \dot{\tau}^{PP} = \dot{\tau}^{PS} \quad \Rightarrow \quad c^P|\nabla\tau^P| = c^S|\nabla\tau^{PS}| \quad \text{and} \quad c^P|\nabla\tau^P| = c^P|\nabla\tau^{PP}|, \tag{5.3}$$

where $c^P = \sqrt{\lambda + 2\mu}$ is the velocity of the P-wave and $c^S = \sqrt{\mu}$ is the velocity of the S-wave.

The partial derivatives along the tangential directions of the boundary can be obtained directly from (5.2). To obtain the momentum component in the reflection direction or the normal direction of the boundary, one needs to use (5.3) and (5.2) together. For example, for the reflection from the P-wave to the S-wave, we have

$$\tau_x^{PS} = -\text{sign}(\tau_x^P)\sqrt{\left(\frac{c^P}{c^S}\right)^2 |\nabla\tau^P|^2 - \left(\tau_y^{PS}\right)^2 - (\tau_z^{PS})^2}. \tag{5.4}$$

Meanwhile, the reflection principle for the momentum component in the normal direction between the same mode, such as P to P or S to S, follows the same way, so we omit it here.

The only ambiguity left here is the case when a beam hits the boundary at a corner. Since a beam hitting a corner causes diffraction, the above beam dynamics does not apply any more. Hence, following [4], we simply ignore the situation when a beam hits a corner of the domain. Since the Gaussian beam method is an asymptotic method and those diffractions have exponentially small effects, the numerical accuracy of beam solutions will not be degraded without those ignored beams.

5.2. P-wave reflecting beams: The Hessian of the phase. To illustrate the derivation of reflected second-order derivatives, we choose three entries among six distinct ones in the Hessian, τ_{yy}, τ_{xy}, and τ_{xx}, since all other entries can be classified into one of these three types. Again, the reflection is assumed to happen along the surface $\{\boldsymbol{x} = (x, y, z) : x = 0\}$ and all terms without arguments are defined at the reflection point.

We start with the first type of reflected derivatives, τ_{yy}. Since it is a tangential component, we have

$$\tau_{yy}^{P} = \tau_{yy}^{PS} = \tau_{yy}^{PP}; \tag{5.5}$$

moreover, τ_{zz} and τ_{yz} will also stay the same.

To derive the second type of reflected derivatives, τ_{xy}^{PS}, we use the partial derivatives with respect to time t so that we have

$$\dot{\tau}_{y}^{P} = c_{y}^{P}|\nabla\tau^{P}| + c^{P}\frac{(\nabla\tau_{y}^{P})^{T}\nabla\tau^{P}}{|\nabla\tau^{P}|}, \tag{5.6}$$

$$\dot{\tau}_{y}^{PS} = c_{y}^{S}|\nabla\tau^{PS}| + c^{S}\frac{(\nabla\tau_{y}^{PS})^{T}\nabla\tau^{PS}}{|\nabla\tau^{PS}|}, \tag{5.7}$$

where we have used the notation $\dot{\tau}_{y} = \frac{\partial^{2}\tau}{\partial t\partial y}$. On the other hand, by the continuity of the tangential and time component of derivatives, we have

$$\dot{\tau}_{y}^{P} = \dot{\tau}_{y}^{PS}. \tag{5.8}$$

Now substituting (5.6) and (5.7) into (5.8) yields

$$\begin{aligned}
c_{y}^{P}|\nabla\tau^{P}| + c^{P}\frac{(\nabla\tau_{y}^{P})^{T}\nabla\tau^{P}}{|\nabla\tau^{P}|} &= c_{y}^{S}|\nabla\tau^{PS}| + c^{S}\frac{(\nabla\tau_{y}^{PS})^{T}\nabla\tau^{PS}}{|\nabla\tau^{PS}|},\\
(\nabla\tau_{y}^{PS})^{T}\nabla\tau^{PS} &= \frac{|\nabla\tau^{PS}|}{c^{S}}\left(c_{y}^{P}|\nabla\tau^{P}| + c^{P}\frac{(\nabla\tau_{y}^{P})^{T}\nabla\tau^{P}}{|\nabla\tau^{P}|} - c_{y}^{S}|\nabla\tau^{PS}|\right),\\
\tau_{xy}^{PS} &= \frac{|\nabla\tau^{PS}|}{c^{S}\tau_{x}^{PS}}\left(c_{y}^{P}|\nabla\tau^{P}| + c^{P}\frac{\nabla\tau_{y}^{P}\cdot\nabla\tau^{P}}{|\nabla\tau^{P}|} - c_{y}^{S}|\nabla\tau^{PS}|\right)\\
&\quad - \frac{1}{\tau_{x}^{PS}}\left(\tau_{y}^{PS}\tau_{yy}^{PS} + \tau_{z}^{PS}\tau_{yz}^{PS}\right).
\end{aligned} \tag{5.9}$$

To obtain the third type of reflected derivatives, τ_{xx}^{PS}, we need to derive the formula of τ_{tx}^{PS} first. We have

$$\dot{\tau}^{P} = c^{P}|\nabla\tau^{P}| \Rightarrow \ddot{\tau}^{P} = c^{P}\frac{(\nabla\dot{\tau}^{P})^{T}\nabla\tau^{P}}{|\nabla\tau^{P}|}, \tag{5.10}$$

$$\dot{\tau}^{PS} = c^{S}|\nabla\tau^{PS}| \Rightarrow \ddot{\tau}^{PS} = c^{S}\frac{(\nabla\dot{\tau}^{PS})^{T}\nabla\tau^{PS}}{|\nabla\tau^{PS}|}. \tag{5.11}$$

We then have the following equation from (5.11) and (5.10):

$$\begin{aligned}
c^{P}\frac{(\nabla\dot{\tau}^{P})^{T}\nabla\tau^{P}}{|\nabla\tau^{P}|} &= c^{S}\frac{(\nabla\dot{\tau}^{PS})^{T}\nabla\tau^{PS}}{|\nabla\tau^{PS}|},\\
(\nabla\dot{\tau}^{PS})^{T}\nabla\tau^{PS} &= \frac{|\nabla\tau^{PS}|}{c^{S}}c^{P}\frac{(\nabla\dot{\tau}^{P})^{T}\nabla\tau^{P}}{|\nabla\tau^{P}|},\\
\dot{\tau}_{x}^{PS} &= \frac{1}{\tau_{x}^{PS}}\left(\frac{|\nabla\tau^{PS}|}{c^{S}}c^{P}\frac{(\nabla\dot{\tau}^{P})^{T}\nabla\tau^{P}}{|\nabla\tau^{P}|} - \dot{\tau}_{y}^{PS}\tau_{y}^{PS} - \dot{\tau}_{z}^{PS}\tau_{z}^{PS}\right).
\end{aligned} \tag{5.12}$$

With the formula of $\dot{\tau}_{x}^{PS}$ given above, τ_{xx}^{PS} can be obtained by solving the following equation:

$$\dot{\tau}^{PS} = c^{S}|\nabla\tau^{PS}| \Rightarrow \dot{\tau}_{x}^{PS} = c_{x}^{S}|\nabla\tau^{PS}| + c^{S}\frac{(\nabla\tau_{x}^{PS})^{T}\nabla\tau^{PS}}{|\nabla\tau^{PS}|}. \tag{5.13}$$

We remark that τ_x^{PS} will not be zero as we have assumed that our initial conditions are compactly supported.

5.3. P-wave reflecting beams: Amplitude vector. We have so far derived the initial conditions of all terms related to the phase function for our new beam dynamics after the P-wave reflection.

Since the phase function itself does not change after reflection at the center of the beam, we have the following equation for the amplitude in order to satisfy the homogeneous boundary condition at the reflection point $\boldsymbol{x}(t^r)$:

$$-a^P \nabla\tau^P = a^{PP}\nabla\tau^{PP} + a^{PS}\boldsymbol{D}^{PS}. \tag{5.14}$$

Since the PS-wave amplitude direction $\boldsymbol{D}^{PS}$ is orthogonal to its ray direction $\nabla\tau^{PS}$ by definition and its norm is one by our construction, the following equation can be obtained if we project both sides of (5.14) to the vector $\nabla\tau^{PS}$:

$$\begin{aligned} -a^P(\nabla\tau^P)^T\nabla\tau^{PS} &= a^{PP}(\nabla\tau^{PP})^T\nabla\tau^{PS}, \\ a^{PP} &= -a^P\frac{(\nabla\tau^P)^T\nabla\tau^{PS}}{(\nabla\tau^{PP})^T\nabla\tau^{PS}}. \end{aligned} \tag{5.15}$$

Meanwhile, $a^{PS}\boldsymbol{D}^{PS}$ is the summation of two S-waves,

$$a^{PS}\boldsymbol{D}^{PS} = \sum_i \alpha_i^{PS}\boldsymbol{D}^{(i)}. \tag{5.16}$$

Similar to the initial condition for the S-wave, we pick the first direction $\boldsymbol{D}^{(1)}$ to be the first column vector of the matrix $I_3 - \boldsymbol{v}\boldsymbol{v}^T$, where $\boldsymbol{v} = \frac{\nabla\tau^{PS}}{|\nabla\tau^{PS}|}$. Then, the second vector $\boldsymbol{D}_2$ will be $\boldsymbol{D}^{(2)} = \boldsymbol{D}^{(1)} \times \boldsymbol{v}$, where $\times$ represents the cross product between two vectors. After normalizing each direction, we can project the residual $-a^P\nabla\tau^P - a^{PP}\nabla\tau^{PP}$ to each direction to obtain the amplitude coefficients, α_i^{PS}.

5.4. S-wave reflecting beams: The phase term. Similar to the P-wave reflection, when an S-wave reflection happens, the total wavefield consists of three different sources, the original S-wave Gaussian beam, a new S-wave beam after reflection, namely, the S-to-S or SS beam, and a new P-wave beam after reflection, namely, the S-to-P or SP beam. Therefore, to satisfy the homogeneous boundary condition, we have the following equation for the S-wave wavepacket at the reflection point $\boldsymbol{x}(t^r)$:

$$-a^S e^{i\tau^S}\boldsymbol{D}^S = a^{SP}e^{i\tau^{SP}}\nabla\tau^{SP} + a^{SS}e^{i\tau^{SS}}\boldsymbol{D}^{SS}. \tag{5.17}$$

After an initial glance at the above equation, the S-wave reflection dynamics seems to be the same as that of the P-wave reflection developed in the last subsection. However, we will find that some significant differences exist between the two reflections.

To begin with, let us still use an S-ray hitting the surface $\{\boldsymbol{x} = (x, y, z) : x = 0\}$ as an example. We then have

$$\tau_y^S = \tau_y^{SS} = \tau_y^{SP}, \tag{5.18}$$

$$\tau_z^S = \tau_z^{SS} = \tau_z^{SP}, \tag{5.19}$$

$$\tau_t^S = \tau_t^{SS} = \tau_t^{SP}, \tag{5.20}$$

$$c^S|\nabla\tau^S| = c^P|\nabla\tau^{SP}|. \tag{5.21}$$

To satisfy all these equations simultaneously, we get

$$\tau_x^{SP} = -\text{sign}(\tau_x^S)\sqrt{\left(\frac{c^S|\nabla\tau^S|}{c^P}\right)^2 - (\tau_y^S)^2 - (\tau_z^S)^2}. \tag{5.22}$$

Since the S-wave velocity $c^S = \sqrt{\mu}$ is smaller than the P-wave velocity $c^P = \sqrt{\lambda + 2\mu}$, this leads to the possibility that the part inside the square root in (5.22) will be negative, or equivalently, τ_x^{SP} can be pure imaginary, inducing exponentially growing waves on one side of the boundary. Therefore, we need to treat the S-wave reflection carefully.

Let us consider the regular situation first, in which case τ_x^{SP} in (5.22) is real. Then the situation is the same as the P-wave reflection as illustrated above, so we omit the derivation here.

The irregular case is when the term τ_x^{SP} is pure imaginary. Consequently, we have

$$\nabla\tau^{SP} = \begin{pmatrix} i\sqrt{-\left(\frac{c^S|\nabla\tau^S|}{c^P}\right)^2 + (\tau_y^S)^2 + (\tau_z^S)^2} \\ \tau_y^S \\ \tau_z^S \end{pmatrix}. \tag{5.23}$$

This phenomenon is called the evanescent wave and the energy will fade away quickly around the boundary in this case. Therefore, there is no need to derive its Hessian due to its negligible energy.

5.5. S-wave reflecting beams: The amplitude vector. Although the evanescent wave fades away quickly, we still include the SP-wave amplitude vector in our derivation so as to make the derivation easier. Moreover, we need the nonzero amplitude vector $\boldsymbol{A}^{SP}$ to satisfy the homogeneous boundary assumption at the reflection point $\boldsymbol{x}(t^r)$. Therefore, we have

$$-a^S\boldsymbol{D}^S = a^{SP}(\text{Re}(\nabla\tau^{SP}) + i\text{Im}(\nabla\tau^{SP})) + a^{SS}\boldsymbol{D}^{SS}. \tag{5.24}$$

To obtain the amplitude vector $\boldsymbol{A}^{SP} = a^{SP}\nabla\tau^{SP}$, we use the fact that the SS-wave amplitude direction $\boldsymbol{D}^{SS}$ is orthogonal to its ray direction $\mathbf{v}$ so that we have from (5.24)

$$\big(\text{Re}(a^{SP})\text{Re}(\nabla\tau^{SP}) - \text{Im}(a^{SP})\text{Im}(\nabla\tau^{SP})\big)\cdot\boldsymbol{v} = -\text{Re}(a^S)\boldsymbol{D}^S\cdot\boldsymbol{v}; \tag{5.25}$$

$$\big(\text{Re}(a^{SP})\text{Im}(\nabla\tau^{SP}) + \text{Im}(a^{SP})\text{Re}(\nabla\tau^{SP})\big)\cdot\boldsymbol{v} = -\text{Im}(a^S)\boldsymbol{D}^S\cdot\boldsymbol{v}. \tag{5.26}$$

The SP-wave amplitude $\boldsymbol{A}^{SP}$ can be obtained by solving the above system. Consequently, the residual $-a^S\boldsymbol{D}^S - a^{SP}\nabla\tau^{SP}$ is now well defined.

Following the same process used in the PS-wave, we can set up the amplitudes and directions easily for the SS-wave.

Notice that after reflection a ray is no longer smooth, which means that Lemma 2.1 is not applicable when a reflection happens. Naturally, one needs to show that after reflection the imaginary part of the Hessian defined above is still positive definite, especially for the PS-wave and the SP-wave. In [4], the authors proved that this is true for the PP-wave and the SS-wave, i.e., the conversion between the same wave mode. The proof for the conversion between different wave modes is provided in Appendix A.

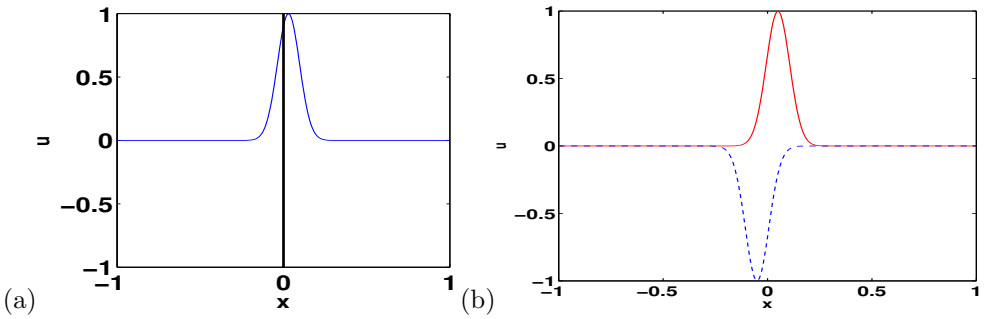

FIG. 2. (a) *Partially reflected beams.* (b) *Partially reflected beams with odd extension.*

5.6. Method of images for boundary conditions. In [4], the authors have proposed a method to tackle the problem caused by partially reflected beams. The partial reflection problem means that the frontier part of a beam is needed to be reflected back even when its central ray has not hit the boundary yet and consequently the reflection dynamics has not been initiated. This is due to the fact that a Gaussian beam has nonzero width, which is illustrated in Figure 2(a).

Therefore, some modifications are needed to treat these partial reflection cases so that the homogeneous boundary condition is satisfied and the wavefield remains continuous. Our strategy is that the outer part will be reflected back into the domain, and this can be realized by an artificial beam. So we essentially apply the odd extension to such a beam as illustrated in Figure 2(b). The trajectory of the blue dashed beam in the figure is completely determined by its counterpart, the red solid beam in the figure, which implies that we do not need any extra assumption of the velocity outside the domain. Therefore, the blue dashed beam only serves as a supplementary beam to satisfy the vanishing boundary condition.

6. Stationary phase analysis of beams. To reinitialize or sharpen a single Gaussian beam, we carry out stationary phase analysis to the single beam. We start with some lemmas and computations which are needed to implement the reinitialization process proposed in section 7.

For any function $u \in L^2(\mathbb{R}^d)$, applying the Fourier–Bros–Iagolnitzer transform [21, 19] allows us to have the following phase-space decomposition of u such that

(6.1)
$$u(\boldsymbol{x}) = \Big(\frac{\omega}{2\pi}\Big)^{3d/2} \int_{R^{3d}} 2^{d/2} e^{i\omega(\boldsymbol{p}(\boldsymbol{x}-\boldsymbol{x}')-\boldsymbol{p}(\tilde{\boldsymbol{x}}-\boldsymbol{x}'))} e^{-\frac{\omega|\boldsymbol{x}-\boldsymbol{x}'|^2}{2}} e^{-\frac{\omega|\tilde{\boldsymbol{x}}-\boldsymbol{x}'|^2}{2}} u(\tilde{\boldsymbol{x}}) d\tilde{\boldsymbol{x}} d\boldsymbol{p} d\boldsymbol{x}',$$

where $\boldsymbol{x}$, $\tilde{\boldsymbol{x}}$, and $\boldsymbol{x}'$ are points in the spatial space $\mathbb{R}^d$, $\boldsymbol{p}$ is the dual momentum variable in the frequency space, and ω is a fixed parameter determining the size of Gaussian window functions.

We will apply the representation (6.1) to Gaussian beams without considering the corresponding amplitude directions so that we can analyze oscillatory properties of Gaussian beams. Using the P-wave as an example, we consider $\Phi^P(t,\boldsymbol{x}) = a(t)e^{i\tau(t,\boldsymbol{x})}$ instead of $a(t)e^{i\tau(t,\boldsymbol{x})}\boldsymbol{p}(t)$.

Moreover, to simplify the stationary phase analysis, we assume that all beam functions considered here depend only on a single variable with other variables being fixed, where the single variable is considered as the principal variable. Therefore, in the following derivations, we take the principal variable to be the variable y, while the other variables, such as x and z, are considered to be fixed.

6.1. Stationary phase analysis with respect to spatial variables. Defined through Gaussian beam evolution, a generic Gaussian wavepacket u can be rewritten with y as the principal variable so that it takes the form

$$u(y;x,z,t) = A(x,z,t)e^{i\Phi(y-y_0)}e^{-\frac{1}{2}\mathrm{Im}(\tau_{yy})(y-y_0^*)^2}, \tag{6.2}$$

where the center of the Gaussian wavepacket is (x_0, y_0, z_0), and all the related beam ingredients are defined at this center if not otherwise specified. Furthermore, y_0^* is a to-be-defined scalar, τ is the phase function, and

$$\begin{aligned}\Phi(y-y_0) = {} & \tau_y(y-y_0) + \frac{\mathrm{Re}(\tau_{yy})(y-y_0)^2}{2} + \mathrm{Re}(\tau_{xy})(y-y_0)(x-x_0) \\ & + \mathrm{Re}(\tau_{zy})(y-y_0)(z-z_0).\end{aligned} \tag{6.3}$$

To define the scalar y_0^*, we use the relation

$$\begin{aligned}&(x-x_0, y-y_0, z-z_0)\begin{pmatrix}\tau_{xx} & \tau_{xy} & \tau_{xz}\\ \tau_{xy} & \tau_{yy} & \tau_{yz}\\ \tau_{xz} & \tau_{zy} & \tau_{zz}\end{pmatrix}\begin{pmatrix}x-x_0\\ y-y_0\\ z-z_0\end{pmatrix} \\ &\quad = \tau_{yy}(y-y_0)^2 + 2(\tau_{xy}(x-x_0)+\tau_{xz}(z-z_0))(y-y_0) + B(x,z) \\ &\quad = \tau_{yy}\left(y-y_0+\frac{\tau_{xy}(x-x_0)+\tau_{xz}(z-z_0)}{\tau_{yy}}\right)^2 + \tilde{B}(x,z),\end{aligned} \tag{6.4}$$

where all second-order derivatives are from the imaginary part of the Hessian of the phase function; consequently, in formula (6.4), $\tilde{B}(x,z)$ is a constant with respect to y, and the complete-square term is defined as $(y-y_0^*)^2$, where

$$y_0^* = y_0 - \frac{\tau_{xy}(x-x_0)+\tau_{xz}(z-z_0)}{\tau_{yy}}. \tag{6.5}$$

To simplify the notation, we denote $R = \mathrm{Re}(\tau_{yy})$ and $I = \mathrm{Im}(\tau_{yy})$ throughout this section. Applying decomposition (6.1) to $u(y;x,z,t)$, we have

$$u(y;x,z,t) = A(x,z,t)\left(\frac{\omega}{2\pi}\right)^{3/2}\int_{R^2}\sqrt{2}e^{i\omega p(y-y')}e^{-\frac{\omega}{2}|y-y'|^2}\psi(p,y')dpdy', \tag{6.6}$$

where

$$\psi(p,y') = e^{i\tilde{B}(x,z)}\int e^{-i\omega p(\tilde{y}-y')}e^{-\frac{\omega}{2}|\tilde{y}-y'|^2}e^{i\Phi(\tilde{y}-y_0)}e^{-\frac{I}{2}|\tilde{y}-y_0^*|^2}d\tilde{y}. \tag{6.7}$$

We will apply the following stationary phase approximation lemma to calculate $\psi(p,y')$.

LEMMA 6.1 (Theorem 7.7.5 in [16]). *Consider the integral*

$$I(\omega) = \int_a^b f(t)e^{i\omega g(t)}dt,$$

where f and g are functions smooth enough to admit Taylor expansions in the interval $[a,b]$, and g is real-valued. Suppose there is a point $c_0 \in [a,b]$ such that $\frac{dg}{dt}(c_0) =$

$g^{'}(c_0) = 0$ *and* $g^{'}(t) \neq 0$ *for* $t \neq c_0$ *in the closed interval* $[a, b]$. *Moreover,* $\frac{d^2g}{dt^2}(c_0) = g^{''}(c_0) \neq 0$. *When* $\omega >> 1$, *the following approximation holds:*

$$I(\omega) = \int_a^b f(t)e^{i\omega g(t)}dt = f(c_0)e^{i\omega g(c_0)}e^{i\pi\delta/4}\sqrt{\frac{2\pi}{\omega|g^{''}(c_0)|}} + O\left(\frac{1}{\omega}\right), \tag{6.8}$$

where δ *is the sign of* $g^{''}(c_0)$.

To use Lemma 6.1, we first substitute $y^{'} = y_0 + ma$ into $u(y; x, z, t)$ in (6.6), where the values of a and ω are to be determined in the following derivation. By (6.7), we have

$$e^{-i\tilde{B}(x,z)}\psi(p, y_0 + ma) = \int e^{i\omega\left(\frac{\Phi(\tilde{y}-y_0)}{\omega} - p(\tilde{y}-y_0-ma)\right)}e^{-\frac{\omega}{2}|\tilde{y}-y_0-ma|^2}e^{-\frac{I}{2}|\tilde{y}-y_0^*|^2}d\tilde{y}. \tag{6.9}$$

To compute the critical point $\tilde{y}_0$ of the phase function $\frac{\Phi(\tilde{y}-y_0)}{\omega} - p(\tilde{y} - y_0 - ma)$, we have

$$\begin{aligned} 0 &= \frac{\Phi^{'}(\tilde{y} - y_0)}{\omega} - p, \\ 0 &= \frac{R(\tilde{y} - y_0) + \mathrm{Re}(\tau_{xy})(x - x_0) + \mathrm{Re}(\tau_{yz})(z - z_0)}{\omega} + \frac{\tau_y}{\omega} - p, \end{aligned} \tag{6.10}$$

yielding

$$\tilde{y}_0 = y_0 + \frac{\omega p - \tau_y - \mathrm{Re}(\tau_{xy})(x - x_0) - \mathrm{Re}(\tau_{yz})(z - z_0)}{R}. \tag{6.11}$$

We denote

$$\begin{aligned} E(x, z) &= \frac{-\mathrm{Re}(\tau_{xy})(x - x_0) - \mathrm{Re}(\tau_{yz})(z - z_0)}{R}, \\ \tilde{y}_0 - y_0 &= \frac{\omega p - \tau_y}{R} + E. \end{aligned} \tag{6.12}$$

Since $E(x, z)$ is independent of the variable y, applying Lemma 6.1 to function $\psi(p, y_0 + ma)$ leads to

$$\begin{aligned} e^{-i\tilde{B}(x,z)}\psi(p, y_0 + ma) = e^{i\omega\left(\frac{\Phi\left(\frac{\omega p-\tau_y}{R}+E\right)}{\omega} - p\left(\frac{\omega p-\tau_y}{R}+E-ma\right)\right)}e^{-\frac{\omega}{2}\left|\frac{\omega p-\tau_y}{R}+E-ma\right|^2} \\ \times e^{-\frac{I}{2}\left|\frac{\omega p-\tau_y}{R}+E-y_0^*+y_0\right|^2}e^{i\frac{\pi}{4}\frac{R}{|R|}}\sqrt{\frac{2\pi}{|R|}}. \end{aligned}$$

Substituting the expression of the term Φ into the above equation, we have

$$\begin{aligned} \psi(p, y_0 + ma) = e^{i\tilde{B}}e^{i\frac{\pi}{4}\frac{R}{|R|}}\sqrt{\frac{2\pi}{|R|}}e^{-\frac{I}{2}\left|\frac{\omega p-\tau_y}{R}-y_0^*+y_0+E\right|^2}e^{-\frac{\omega}{2}\left|\frac{\omega p-\tau_y}{R}+E-ma\right|^2} \\ \times e^{i\omega\left(\frac{\tau_y}{\omega}\left(\frac{\omega p-\tau_y}{R}+E\right)-\left(\frac{R\cdot E}{\omega}\right)\left(\frac{\omega p-\tau_y}{R}+E\right)-p\left(\frac{\omega p-\tau_y}{R}+E-ma\right)+\frac{R}{2\omega}\left(\frac{\omega p-\tau_y}{R}+E\right)^2\right)}. \end{aligned} \tag{6.13}$$

Inserting the expression (6.13) into (6.6), we obtain

$$\begin{aligned} u(y;x,z,t) &= aA(x,z,t)\sqrt{\Big(\frac{\omega}{2\pi}\Big)^3}\int \sqrt{2}e^{i\omega p(y-y_0-ma)}e^{-\frac{\omega}{2}|y-y_0-ma|^2}\psi(\cdot,\cdot)dpdm \\ &\approx 2Aa\sqrt{\Big(\frac{\omega}{2\pi}\Big)^3}\sqrt{\frac{\pi}{|R|}}e^{i\frac{\pi}{4}\frac{R}{|R|}}e^{i\tilde{B}}\int e^{i\omega p(y-y_0-ma)}e^{-\frac{\omega}{2}|y-y_0-ma|^2} \\ &\quad\times e^{-\frac{\omega}{2}\left|\frac{\omega p-\tau_y}{R}+E-ma\right|^2}e^{i\omega\left(\frac{\tau_y}{\omega}\left(\frac{\omega p-\tau_y}{R}+E\right)-\frac{R\cdot E}{\omega}\left(\frac{\omega p-\tau_y}{R}+E\right)-p\left(\frac{\omega p-\tau_y}{R}+E-ma\right)\right)} \\ &\quad\times e^{-\frac{I}{2}\left|\frac{\omega p-\tau_y}{R}-y_0^*+y_0+E\right|^2}e^{i\frac{R}{2}\left(\frac{\omega p-\tau_y}{R}+E\right)^2}dpdm. \end{aligned} \tag{6.14}$$

Therefore, by applying the stationary phase approximation to the variable $\tilde{y}$, we have reduced the triple integral (6.1) to the double integral (6.14).

Applying Lemma 6.1 requires that $R \neq 0$. However, if $R = 0$, then the integral about the function $\psi(p, y^{'})$ is nothing but the Fourier transform of a Gaussian function about y, and the situation is trivial.

6.2. Stationary phase analysis with respect to momenta. Starting from the double integral (6.14), we apply the stationary phase approximation again, and this time we will apply the analysis to the momentum variable p.

We have

$$\begin{aligned} u(y;x,z,t) &= A(x,z,t)e^{i\tilde{B}}\sqrt{\Big(\frac{\omega}{2\pi}\Big)^3}\sqrt{\frac{4\pi}{|R|}}e^{i\frac{\pi}{4}\frac{R}{|R|}}a\int e^{-\frac{\omega}{2}|y-y_0-ma|^2}dm \\ &\quad\times\int e^{i\omega p(y-y_0-ma)}e^{-\frac{I}{2}\left|\frac{\omega p-\tau_y}{R}-y_0^*+y_0+E\right|^2}e^{-\frac{\omega}{2}\left|\frac{\omega p-\tau_y}{R}+E-ma\right|^2} \\ &\quad\times e^{i\omega\left(\frac{\tau_y}{\omega}\left(\frac{\omega p-\tau_y}{R}+E\right)-\frac{R\cdot E}{\omega}\left(\frac{\omega p-\tau_y}{R}+E\right)-p\left(\frac{\omega p-\tau_y}{R}+E-ma\right)+\frac{R}{2\omega}\left(\frac{\omega p-\tau_y}{R}+E\right)^2\right)}dp. \end{aligned} \tag{6.15}$$

For the inner integral of (6.15), the phase function $g(p)$ is

$$\begin{aligned} g(p) &= p(y-y_0-ma)+\frac{\tau_y}{\omega}\left(\frac{\omega p-\tau_y}{R}+E\right) \\ &\quad-\frac{R\cdot E}{\omega}\left(E+\frac{\omega p-\tau_y}{R}\right)-p\left(E-ma+\frac{\omega p-\tau_y}{R}\right)+\frac{R}{2\omega}\left(\frac{\omega p-\tau_y}{R}+E\right)^2, \end{aligned}$$

and the smooth function $f(p)$ is

$$f(p) = e^{-\frac{\omega}{2}\left|\frac{\omega p-\tau_y}{R}+E-ma\right|^2}e^{-\frac{I}{2}\left|\frac{\omega p-\tau_y}{R}-y_0^*+y_0+E\right|^2}. \tag{6.16}$$

To compute the critical point, we set $g^{'}(p) = 0$, where

$$g^{'}(p) = y-y_0-ma+\frac{\tau_y}{R}-E-\left(E-ma+\frac{\omega p-\tau_y}{R}\right)-\frac{p\omega}{R}+\left(\frac{\omega p-\tau_y}{R}+E\right). \tag{6.17}$$

It follows that the critical point p_0 satisfies

$$\begin{aligned} &\frac{\omega p}{R} = y-y_0-E+\frac{\tau_y}{R} \\ &\Rightarrow p_0 = \frac{R}{\omega}(y-y_0-E)+\frac{\tau_y}{\omega} \\ &\Rightarrow \frac{\omega p_0-\tau_y}{R} = y-y_0-E. \end{aligned} \tag{6.18}$$

The second-order derivative of the phase function g at the critical point p_0 is

$$g''(p_0) = -\frac{\omega}{R}. \tag{6.19}$$

Therefore, the approximation of the inner integral of formula (6.15) is

$$\begin{aligned}
&\int e^{i\omega p(y-y_0-ma)} e^{-\frac{I}{2}\left|\frac{\omega p-\tau_y}{R}-y_0^*+y_0+E\right|^2} e^{-\frac{\omega}{2}\left|\frac{\omega p-\tau_y}{R}+E-ma\right|^2} \\
&\quad\times e^{i\omega\left(\frac{\tau_y}{\omega}\left(\frac{\omega p-\tau_y}{R}+E\right)-\frac{R\cdot E}{\omega}\left(\frac{\omega p-\tau_y}{R}+E\right)-p\left(\frac{\omega p-\tau_y}{R}+E-ma\right)+\frac{R}{2\omega}\left(\frac{\omega p-\tau_y}{R}+E\right)^2\right)} dp \\
&= \sqrt{\frac{\pi R}{\omega^2}} e^{-i\frac{\pi R}{4|R|}} e^{i\omega p_0(y-y_0-ma)} e^{-\frac{I}{2}|y-y_0^*|^2} e^{-\frac{\omega}{2}|y-y_0-ma|^2} \\
&\quad\times e^{i\omega\left((y-y_0)\left(\frac{\tau_y-R\cdot E}{\omega}\right)\right)} e^{i\omega\left(-p_0(y-y_0-ma)+\frac{R}{2\omega}(y-y_0)^2\right)}.
\end{aligned}$$

We summarize the results of the stationary-phase analysis into the following lemma.

LEMMA 6.2. *Suppose the principal variable selected for the function $u(y;x,z,t)$ is y,*

$$u(y;x,z,t) = A(x,z,t)e^{i\Phi(y-y_0)}e^{-\frac{1}{2}\mathrm{Im}(\tau_{yy})(y-y_0^*)^2}, \tag{6.20}$$

$R = \mathrm{Re}(\tau_{yy})$ is nonzero, and $I = \mathrm{Im}(\tau_{yy})$. Then there exists ω in the order of $O(I)$ such that the following decomposition holds:

$$\begin{aligned}
u(y;x,z,t) &= aA(x,z,t)e^{i\tilde{B}(x,z)}\sqrt{\frac{\omega}{2\pi}} \\
&\quad\times \int e^{-\omega|y-y_0-ma|^2} e^{-\frac{I}{2}|y-y_0^*|^2} e^{i\tilde{\tau}_y(y-y_0)} e^{i\frac{R}{2}(y-y_0)^2} dm + O\left(\frac{1}{\omega}\right),
\end{aligned} \tag{6.21}$$

where $\tilde{\tau}_y = \tau_y - R\times E$ with $R\times E = -\mathrm{Re}(\tau_{xy})(x-x_0) - \mathrm{Re}(\tau_{yz})(z-z_0)$, and the fixed parameter a is defined as $a = \frac{1}{\sqrt{I}}$.

7. Sharpening beams by reinitialization. In this section, we propose a new reinitialization strategy based on Lemma 6.2. Again, we base our analysis on the assumption that the variable y is the principal variable. We first illustrate the reason why it is necessary to propose a new reinitialization strategy.

7.1. The first motivation for new reinitialization strategy. It is necessary to add a reinitialization process into the Gaussian beam propagation since the width of a beam will increase exponentially in a generic medium [24]. We use the one-way 1-D acoustic wave equation with a linear velocity as an example. Suppose $c(x) = \alpha + \beta x$, where α and β are constants. Then the Ricatti equation for the Hessian M becomes

$$\frac{dM}{dt} + 2M\beta = 0, \quad M(0) = i\epsilon. \tag{7.1}$$

Solving this simple linear ODE, we have

$$M(t) = i\epsilon e^{-2\beta t}. \tag{7.2}$$

If the slope $\beta > 0$, then the width of the beam solution will be exponentially increasing; consequently, the beam solution will lose its localization and hence its accuracy in this simple linear velocity model. Since each smooth velocity can be approximated by a linear function locally, the same phenomenon can be expected in other situations.

7.2. The second motivation for new reinitialization strategy. The second motivation is to resolve some issues caused by reflecting beams. Although the reflection formulas that we have derived in section 5 are theoretically correct, it is not trouble free to implement those numerically. In particular, the S-wave reflection induces the SP-wave which may exhibit grazing behaviors in terms of ray theory and Gaussian beams.

To simplify the explanation, we use the 2-D elastic-wave case to illustrate this. Suppose a ray hits the line $\{\boldsymbol{x} = (x, y) : x = 0\}$. Then, according to the analysis in section 5, the y-component of the ray direction τ_y does not change. For the PS reflection, we have

$$\begin{aligned} (c^S \tau_x^{PS})^2 &= (c^P \tau_x^P)^2 + \left((c^P)^2 - (c^S)^2\right) \tau_y^2, \\ (\tau_x^{PS})^2 &= \frac{(\lambda + 2\mu)(\tau_x^P)^2 + (\lambda + \mu)\tau_y^2}{(c^S)^2}, \end{aligned} \tag{7.3}$$

while for the SP reflection, we have

$$(\tau_x^{SP})^2 = \frac{\mu(\tau_x^S)^2 - (\lambda + \mu)\tau_y^2}{(c^P)^2}. \tag{7.4}$$

We then compute the angles θ^{PS} and θ^{SP} between the ray direction and the reflecting boundary $\{\boldsymbol{x} = (x, y) : x = 0\}$, so that we have

$$\begin{aligned} \tan(\theta^{PS}) &= \frac{\tau_x^{PS}}{\tau_y^{PS}} \\ &= \sqrt{\frac{(\lambda + 2\mu)(\tau_x^P)^2 + (\lambda + \mu)\tau_y^2}{(c^S)^2 \tau_y^2}} \\ &= \sqrt{\frac{\lambda + \mu}{\mu} + \frac{(\lambda + 2\mu)(\tau_x^P)^2}{\mu \tau_y^2}}, \end{aligned} \tag{7.5}$$

and

$$\tan(\theta^{SP}) = \sqrt{\frac{\mu(\tau_x^S)^2}{(\lambda + 2\mu)\tau_y^2} - \frac{\lambda + \mu}{\lambda + 2\mu}}. \tag{7.6}$$

We claim that for the PS reflection, the angle between the ray direction and the boundary will increase after reflection, while for the SP reflection, this value will decrease. To see this, for the PS reflection we have

$$\begin{aligned} \left(\frac{\tan(\theta^{PS})}{\tan(\theta^P)}\right)^2 &= \frac{\frac{\lambda+\mu}{\mu} + \frac{(\lambda+2\mu)|\tau_x^P|^2}{\mu\tau_y^2}}{\left(\frac{\tau_x^P}{\tau_y}\right)^2} \\ &= \frac{\lambda + 2\mu}{\mu} + \frac{\lambda + \mu}{\mu}\left(\frac{\tau_y}{\tau_x^P}\right)^2, \end{aligned} \tag{7.7}$$

and for the SP reflection we have

$$\left(\frac{\tan(\theta^{SP})}{\tan(\theta^S)}\right)^2 = \frac{\mu}{\lambda + 2\mu} - \frac{\lambda + \mu}{\lambda + 2\mu}\left(\frac{\tau_y}{\tau_x^S}\right)^2. \tag{7.8}$$

As we can see from (7.7) and (7.8), as τ_y increases or the incidence angle decreases, the ratio for the PS reflection increases, which means that the angle after reflection is

larger than the incidence angle. On the other hand, as τ_y increases, the ratio for the SP reflection decreases as a quadratic function of τ_y, which means that the angle θ^{SP} for the SP-wave will be close to zero even when the incoming S-wave's incidence angle θ is away from zero; consequently, if θ^{SP} is close to zero, then the resulting grazing beam with larger width will interact significantly with the boundary, and such a beam needs sharpening so as to have a well-behaved beam.

We make the following comments. Since no wave-mode conversion occurs in the acoustic wave propagation, it is relatively easy to handle beam reflection of acoustic waves as illustrated in [4]. However, as illustrated in the above and the following numerical experiments, it is much harder to deal with beam reflection of elastic waves as wave-mode conversions do occur in the elastic wave propagation.

7.3. Sharpening wavepackets and convergence analysis. By Lemma 6.2, we have

(7.9)
$$u(y) = aAe^{i\tilde{B}}\sqrt{\frac{\omega}{2\pi}}e^{-\frac{I}{2}|y-y_0^*|^2}e^{i\tilde{\tau}_y(y-y_0)}e^{i\frac{R}{2}(y-y_0)^2}\int e^{-\omega|y-y_0-ma|^2}dm + O\left(\frac{1}{\omega}\right),$$

where the term $\tilde{\tau}_y$ is the modified y-direction of the central ray and is equal to

$$\tilde{\tau}_y = \tau_y - R \times E. \tag{7.10}$$

To sharpen Gaussian wavepackets, we have the following lemma.

LEMMA 7.1. *Assume that Lemma 6.2 holds. Then there exist parameters ω_k and q such that the following approximation holds:*

$$u(y) \approx aAe^{i\tilde{B}}\sqrt{\frac{\omega}{2\pi}}\sum_{k=0}^{q} l_k e^{i\tilde{\tau}_y(y-y_0)}e^{-\omega_k|y-y_0^*|^2}e^{-\frac{I}{2}|y-y_0^*|^2}e^{i\frac{R}{2}(y-y_0)^2}, \tag{7.11}$$

where $a = \frac{1}{\sqrt{I}}$.

As we can see, the extra term $e^{-\omega_k|y-y_0^*|^2}$ reduces the size of beams, where positive parameters ω_k are obtained by choosing the parameter ω in Lemma 6.2 appropriately.

Proof. To obtain (7.11), we first rewrite

$$\begin{aligned}\int e^{-\omega|y-y_0-ma|^2}dm &= \int e^{-\omega|y-y_0^*+y_0^*-y_0-ma|^2}dm\\ &= \int e^{-\omega|y-y_0^*|^2}e^{-\omega|y_0^*-y_0-ma|^2}e^{-2\omega(y-y_0^*)(y_0^*-y_0-ma)}dm\\ &= e^{-\omega|y-y_0^*|^2}\int e^{-\omega|y_0^*-y_0-ma|^2}e^{-2\omega(y-y_0^*)(y_0^*-y_0-ma)}dm. \qquad (7.12)\end{aligned}$$

The integral in (7.12) can be further reduced so that we have

$$\begin{aligned}&\int e^{-\omega|y_0^*-y_0-ma|^2}e^{-2\omega(y-y_0^*)(y_0^*-y_0-ma)}dm\\ &= \sum_{\tilde{k}}\int_{\tilde{k}-\frac{1}{2}}^{\tilde{k}+\frac{1}{2}} e^{-\omega|y_0^*-y_0-ma|^2}e^{-2\omega(y-y_0^*)(y_0^*-y_0-ma)}dm\\ &= \sum_{k\in\mathbb{Z}}\int_{-\frac{1}{2}}^{\frac{1}{2}} e^{-\omega|(k+\delta)a|^2}e^{2\omega(y-y_0^*)((k+\delta)a)}d\delta, \qquad (7.13)\end{aligned}$$

where we require k to be integers so that $\tilde{k}$ satisfies $k = \tilde{k} + \frac{y_0-y_0^*}{a}$.

Since $e^{-\omega|y-y_0-ma|^2}$ is an L_1 function, we can truncate the above summation to a finite number of terms, $|k| \le q$, where q is a fixed positive integer. By the monotone convergence theorem, we have

$$\lim_{N\to\infty} \int_N^{\infty} e^{-\omega|y-y_0-ma|^2} dm = 0. \tag{7.14}$$

We further consider two cases: Case 1, $k = 0$, and Case 2, $k \neq 0$.

Case 1: $k = 0$. In this case, we have

$$\begin{aligned}
\int_{-\frac{1}{2}}^{\frac{1}{2}} e^{-\omega|(k+\delta)a|^2} e^{2\omega(y-y_0^*)((k+\delta)a)} d\delta &= \int_{-\frac{1}{2}}^{\frac{1}{2}} e^{-\omega|\delta a|^2} e^{2\omega(y-y_0^*)(\delta a)} d\delta \\
&\approx \int_{-\frac{1}{2}}^{\frac{1}{2}} e^{-\omega|\delta a|^2} \left(\sum_n \frac{2^n \omega^n (y-y_0^*)^n (\delta a)^n}{n!} \right) d\delta \\
&\approx \int_{-\frac{1}{2}}^{\frac{1}{2}} e^{-\omega|\delta a|^2} \left(\sum_n \frac{(2\omega)^{2n} (y-y_0^*)^{2n} (\delta a)^{2n}}{(2n)!} \right) d\delta, \qquad (7.15)
\end{aligned}$$

where the odd power terms in δ vanish in the last step above since the integral of an odd function in $[-\frac{1}{2}, \frac{1}{2}]$ is zero. Here $e^{-\omega|\delta a|^2}$ is an even function about δ and all odd power functions are odd functions.

Therefore, we have

$$\begin{aligned}
\int_{-\frac{1}{2}}^{\frac{1}{2}} e^{-\omega|\delta a|^2} e^{2\omega(y-y_0^*)(\delta a)} d\delta &\approx \int_{-\frac{1}{2}}^{\frac{1}{2}} e^{-\omega|\delta a|^2} \left(1 + 2\omega^2 (y-y_0^*)^2 (\delta a)^2\right) d\delta \\
&\approx \int_{-\frac{1}{2}}^{\frac{1}{2}} e^{-\omega|\delta a|^2} e^{2\omega^2 (y-y_0^*)^2 (\delta a)^2} d\delta, \qquad (7.16)
\end{aligned}$$

where the leading order error from (7.16) is $O(\frac{(2\omega)^4 (y-y_0^*)^4 (\delta a)^4}{4!})$.

Case 2: $k \neq 0$. When $k < 0$, by setting $\tilde{\delta} = -\delta$, we have

$$\begin{aligned}
\int_{-\frac{1}{2}}^{\frac{1}{2}} e^{-\omega|(k+\delta)a|^2} e^{2\omega(y-y_0^*)((k+\delta)a)} d\delta &= \int_{-\frac{1}{2}}^{\frac{1}{2}} e^{-\omega|-|k|a+\delta a|^2} e^{2\omega(y-y_0^*)(-|k|a+\delta a)} d\delta \\
&= \int_{-\frac{1}{2}}^{\frac{1}{2}} e^{-\omega|-|k|a-\tilde{\delta} a|^2} e^{2\omega(y-y_0^*)(-|k|a-\tilde{\delta} a)} d\tilde{\delta} \\
&= \int_{-\frac{1}{2}}^{\frac{1}{2}} e^{-\omega||k|a+\delta a|^2} e^{-2\omega(y-y_0^*)(|k|a+\delta a)} d\delta. \qquad (7.17)
\end{aligned}$$

When $k > 0$, we have

$$\int_{-\frac{1}{2}}^{\frac{1}{2}} e^{-\omega|(k+\delta)a|^2} e^{2\omega(y-y_0^*)((k+\delta)a)} d\delta = \int_{-\frac{1}{2}}^{\frac{1}{2}} e^{-\omega|(|k|+\delta)a|^2} e^{2\omega(y-y_0^*)((|k|+\delta)a)} d\delta. \tag{7.18}$$

Given $k > 0$, we add (7.18) for $k > 0$ and (7.17) for $-k < 0$, so that we have

$$\begin{aligned}
&\int_{-\frac{1}{2}}^{\frac{1}{2}} e^{-\omega|ka+\delta a|^2} \left(e^{2a\omega(y-y_0^*)(k+\delta)} + e^{-2a\omega(y-y_0^*)(k+\delta)} \right) d\delta \\
&= \int_{-\frac{1}{2}}^{\frac{1}{2}} 2e^{-\omega|ka+\delta a|^2} \left(1 + 2\omega^2 (y-y_0^*)^2 (k+\delta)^2 a^2\right) d\delta, \qquad (7.19)
\end{aligned}$$

where we have used Taylor expansions of the exponential functions. Furthermore, we have

$$\int_{-\frac{1}{2}}^{\frac{1}{2}} 2e^{-\omega|ka+\delta a|^2}\left(1+2\omega^2(y-y_0^*)^2(k+\delta)^2a^2\right)d\delta$$

$$\approx \int_{-\frac{1}{2}}^{\frac{1}{2}} 2e^{-\omega(k+\delta)^2a^2}e^{2\omega^2(y-y_0^*)^2((k+\delta)a)^2}d\delta, \tag{7.20}$$

where the error term is $O(\frac{(2\omega)^4(y-y_0^*)^4(\delta a+ka)^4}{4!})$.

The errors of approximations in (7.20) and (7.16) can be summarized in a unified form, i.e., $O(\frac{(2\omega)^4(y-y_0^*)^4(\delta a+ka)^4}{4!})$.

Now the integral (7.13) becomes

$$\int e^{-\omega|y_0^*-y_0-ma|^2}e^{-2\omega(y-y_0^*)(y_0^*-y_0-ma)}dm = \int_{-\frac{1}{2}}^{\frac{1}{2}} e^{-\omega|\delta a|^2}e^{-2\omega(y-y_0^*)(\delta a)}d\delta$$

$$+\sum_{k>0}\int_{-\frac{1}{2}}^{\frac{1}{2}} 2e^{-\omega(k+\delta)^2a^2}e^{2\omega^2(y-y_0^*)^2((k+\delta)a)^2}d\delta. \tag{7.21}$$

To compute l_k and ω_k, we start with the sum of $k>0$ so that we have

$$e^{-\omega|y-y_0^*|^2}\int_{-\frac{1}{2}}^{\frac{1}{2}} 2e^{-\omega(k+\delta)^2a^2}e^{2\omega^2(y-y_0^*)^2((k+\delta)a)^2}d\delta$$

$$\approx 2e^{-\omega|y-y_0^*|^2}e^{2\omega^2(y-y_0^*)^2(ka)^2}e^{-\omega|ka|^2}$$

$$= l_k e^{-\omega|y-y_0^*|^2}e^{2\omega^2(y-y_0^*)^2(ka)^2}, \tag{7.22}$$

where the first step above is obtained by choosing $\delta=0$. Accordingly, we define l_k by

$$l_k = 2e^{-\omega|ka|^2}. \tag{7.23}$$

Similarly, for the term with $k=0$, we have

$$l_k = 1. \tag{7.24}$$

Next we choose the parameter ω and define ω_k accordingly. We start with making the exponent in (7.22) negative,

$$-\omega+2\omega^2k^2a^2\le 0 \quad\Rightarrow\quad \omega\le\frac{1}{2a^2k^2} \quad \text{for} \quad k=1,2,\dots,q, \tag{7.25}$$

where q is the truncation parameter for the exponential integral as used in (7.14), and a is previously defined as $\frac{1}{\sqrt{I}}$ in Lemma 6.2.

If we choose $\omega=\frac{I}{3q^2}$, then ω_k in (7.11) is defined by

$$\omega_k = \omega-2\omega^2(ka)^2 = \left(\frac{3q^2-2k^2}{9q^4}\right)I. \tag{7.26}$$

Having defined l_k and ω_k, we now characterize the size of the error term so that we have

$$\max_{k\le q}\frac{(2\omega)^4(y-y_0^*)^4(\delta a+ka)^4}{4!}=\frac{(2\omega)^4(y-y_0^*)^4(\delta a+qa)^4}{4!}$$

$$\le\frac{2}{3}\left(\frac{I}{3q^2}\right)^4\left(\frac{1}{\sqrt{I}}\right)^4(qa)^4\le\frac{2}{243}\frac{1}{q^4}. \tag{7.27}$$

Although the above is only the leading-order term in the series we truncated, the rest of the series is easily controlled from the following two considerations: the first consideration is that the rest of the series have higher power about q, i.e., $\frac{1}{q^{2n}}$, for $n = 3, 4, \ldots$; the second consideration is that the coefficients $\frac{2^{2n}}{(2n)!}$ decay exponentially. ∎

7.4. Complexity analysis. Following the complexity analysis in [24, 4], we now analyze the computational complexity of the overall algorithm, which consists of three parts. The first part is due to the initialization step by the multiscale vectorial Gaussian wavepacket transform, which has complexity $O(N^d \log N)$, where N is the total number of points in each spatial dimension. The second part is due to the propagation step of all the Gaussian beams. Since the Gaussian beam equations themselves do not contain the large frequency parameter, integrating each beam over a finite time period takes $O(1)$ steps, and the total cost for this part is proportional to the total number of beams. The final part is due to the summation step; as the support of each Gaussian beam is of size $O(N^{1/2})$ in each dimension, each beam at time T covers about $O(N^{d/2})$ points. Overall, the computational complexity of the entire algorithm is $O(N^d \log N + C \cdot N^{d/2})$, where C denotes the number of beams being traced. However, for all usual initial conditions, such as point sources, plane waves, and curvilinear wavefronts, the multiscale Gaussian wavepackets provide theoretically sparse approximations to these initial conditions, following an argument similar to the ones in [26, 8, 12]. Most importantly, such sparsity is preserved throughout the time evolution. Therefore, for such initial conditions, the number of beams would always be small. Under such situations, our complexity of $O(N^d \log N + C \cdot N^{d/2})$ is much more efficient compared to the $O(N^{d+1})$ cost of standard finite difference or finite element methods.

8. Numerical examples. We present numerical examples to justify our new method for 3-D elastic wave equations. We will use numerical solutions computed by the finite-difference time-domain (FDTD) method on staggered grids [27] as reference solutions to validate our computational results. The 3-D FDTD method is implemented in the C language, and the resulting codes are further accelerated by using GPUs.

All the 3-D examples are posed on the same spatial computational domain which is $[0, 0.5]^3$. The terminal time T will be specified in individual cases. To have reliable, accurate FDTD solutions to compare with, we have to mitigate dispersion errors of the finite-difference method [6, 3]. Therefore, we use a very fine mesh for the FDTD method, where a mesh size of $\frac{1}{640}$ in each spatial direction is prescribed to compute numerical solutions; this mesh size seems to suffice for the purpose of our numerical comparisons shown here.

8.1. Beam reinitialization.

8.1.1. S-to-P reflection versus P-to-S reflection. We provide numerical results to justify our analysis carried out in sections 7.2 and 7.3.

To start with, we conduct the following experiments to illustrate the difference between the S-to-P reflection and the P-to-S reflection. The elastic parameters are taken to be $\lambda = \mu = 1$.

The pure S-wave initial conditions for the experiment are $\boldsymbol{g}^S = \mathbf{0}$ and

(8.1)
$$\boldsymbol{f}^S = \begin{pmatrix} -\sin(\alpha)\sin(36\pi x + 36\pi\sin(\alpha)(y-0.25))e^{-36\pi^2\left(x^2+(y-0.25)^2+(z-0.25)^2\right)} \\ \sin(36\pi x + 36\pi\sin(\alpha)(y-0.25))e^{-36\pi^2\left(x^2+(y-0.25)^2+(z-0.25)^2\right)} \\ 0 \end{pmatrix},$$

so that the initial width of beams is set to be $36\pi^2$.

The pure P-wave initial conditions for the experiment are $\boldsymbol{g}^P = \mathbf{0}$ and

$$\boldsymbol{f}^P = \begin{pmatrix} \sin(36\pi x + 36\pi\sin(\alpha)(y-0.25))e^{-36\pi^2\left(x^2+(y-0.25)^2+(z-0.25)^2\right)} \\ \sin(\alpha)\sin(36\pi x + 36\pi\sin(\alpha)(y-0.25))e^{-36\pi^2\left(x^2+(y-0.25)^2+(z-0.25)^2\right)} \\ 0 \end{pmatrix},$$

so that the initial width of beams is set to be $36\pi^2$ as well.

Figure 3 shows the results, in which the red-star line is the ratio $\frac{\sin(\theta^{PS})}{\sin(\alpha)}$, and the blue line is the ratio $\frac{\sin(\theta^{SP})}{\sin(\alpha)}$. As analyzed in section 7.2, the angle for the SP reflection decreases to zero when the incident hitting angle increases. Therefore, the SP reflection beams will be sharpened so that they become more localized.

8.1.2. Sharpened beams versus original beams. We use an example to demonstrate that beam accuracy will not be negatively impacted after adding the new reinitialization process (7.11). Therefore, we compare the computed wavefield obtained with reinitialization with that without reinitialization. By Lemma 7.1, we will choose the truncation parameter $q = 2$ according to (7.27) in our reinitialization process.

Suppose an S-wave beam hits the boundary $x = 0$ at the central point $(0, 0.1, 0.1)$, where its Hessian equals

$$\begin{pmatrix} 36\pi + 36\pi^2 i & 12\pi^2 i & 0 \\ 12\pi^2 i & 7\pi^2 + 36\pi^2 i & 0 \\ 0 & 0 & 4\pi^2 + 36\pi^2 i \end{pmatrix},$$

and the norm of its amplitude vector is set to be 100.

In Figure 4, we show wavefields along two different lines, $(0 \le x \le 0.5, 0.1, 0.1)$ and $(0 \le x \le 0.5, 0.08, 0.13)$, to validate our reinitialization strategy. As we can see, the reinitialization strategy will not affect accuracy of the overall results, but the width of each new beam has been decreased.

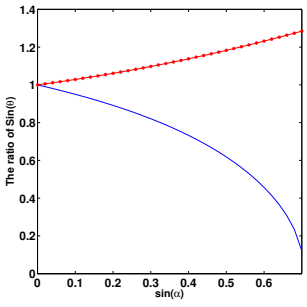

FIG. 3. *P-to-S reflection versus S-to-P reflection with different behavior of angle ratios, where P-to-S: "*"; S-to-P: "-".*

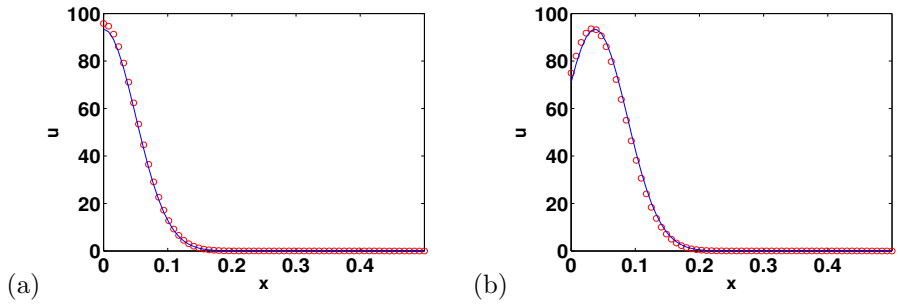

FIG. 4. *Sharpened beams versus original beams.* (a) $(0 \le x \le 0.5, y = 0.1, z = 0.1)$. (b) $(0 \le x \le 0.5, y = 0.08, z = 0.13)$. *Solution with reinitialization: "o"; solution without reinitialization: "-".*

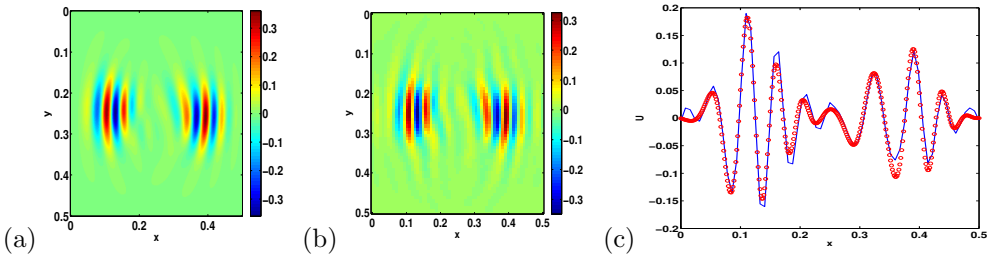

FIG. 5. *Example* 1. *Generic initial values with periodic boundary conditions.* (a) *FDTD on* $z = 0.25$ *at* $T = 0.14$. (b) *Gaussian beam on* $z = 0.25$ *at* $T = 0.14$. (c) *The line comparison along the x-direction, where* $z = 0.25$ *and* $y = \frac{6}{32}$*; FDTD: "o"; Gaussian beam: "-".*

8.2. Periodic boundary conditions. We show some numerical results for treating periodic boundary conditions.

8.2.1. Example 1. General initial conditions in a uniform medium. We further test our algorithm on a homogeneous model with constant elastic moduli $\lambda = \mu = 1$, and the initial conditions are taken to be $\boldsymbol{g} = 0$ and

$$\boldsymbol{f} = \begin{pmatrix} \sin(72\pi x^2) e^{-36\pi^2\left((x-0.25)^2+(z-0.25)^2+(z-0.25)^2\right)} \\ \sin(72\pi x^2) e^{-36\pi^2\left((x-0.25)^2+(z-0.25)^2+(z-0.25)^2\right)} \\ 0 \end{pmatrix}. \tag{8.2}$$

Figure 5 shows comparison results. As we can see, the Gaussian beam result is comparable to the FDTD result in the asymptotic or high-frequency regime, and some asymptotic errors only appear in the place where the wavefield is very weak.

8.3. Dirichlet boundary conditions: Pure P-wave initial conditions. We now deal with the Dirichlet boundary conditions. We first check our reflection mechanism for pure P-wave initial conditions. We choose the initial conditions as the following:

$$\boldsymbol{f} = \begin{pmatrix} \sin(32\pi x + 8\pi y) e^{-36\pi^2\left((x-0.15)^2+(y-0.25)^2+(z-0.25)^2\right)} \\ \frac{1}{4}\sin(32\pi x + 8\pi y) e^{-36\pi^2\left((x-0.15)^2+(y-0.25)^2+(z-0.25)^2\right)} \\ 0 \end{pmatrix} \tag{8.3}$$

and

$$\boldsymbol{g} = \begin{pmatrix} 2\sin(32\pi x + 8\pi y)e^{-36\pi^2\left((x-0.15)^2+(y-0.25)^2+(z-0.25)^2\right)} \\ \frac{1}{2}\sin(32\pi x + 8\pi y)e^{-36\pi^2\left((x-0.15)^2+(y-0.25)^2+(z-0.25)^2\right)} \\ 0 \end{pmatrix}. \tag{8.4}$$

The reason that we choose to start with pure P-wave initial conditions is that we can easily validate our P-wave reflection mechanism as both P-to-P and P-to-S wave modes will occur in the process.

8.3.1. Example 2. P-wave reflection in a sinusoidal model. We choose elastic parameters $\lambda = 1 + \sin(4\pi x)$ and $\mu = 2$, which may induce caustics in wave propagation. Figure 6 shows the computational results at $T = 0.14$. As we can see, the Gaussian beam solution matches with the FDTD solution in a large scale, and some asymptotic errors only appear in the place where the wavefield is very weak.

We remark that the reinitialization scheme is not involved in the P-wave reflection shown above. Small asymptotic errors imply that the P-wave reflection does not require reinitialization.

8.4. Dirichlet boundary conditions: Pure S-wave initial conditions. We have designed a new reinitialization process to deal with the S-wave reflection. In this subsection, we will test this reinitialization process, but first we will justify the necessity of adding this reinitialization process.

Since both S-to-S and S-to-P wave modes will occur in the process of propagating pure S-wave initial conditions, we choose to deal with pure S-wave initial conditions so that we can easily validate our S-wave reflection mechanism.

By Lemma 7.1, we will choose the truncation parameter $q = 2$ according to (7.27) in the reinitialization process when needed.

8.4.1. Example 3. S-wave reflection with vertical hitting angle. We check the S-wave reflection with a vertical hitting angle, that is, the case $\sin(\alpha) = 0$ in Figure 3. We choose elastic parameters to be $\lambda = 1$ and $\mu = 2$. We take the initial conditions to be $\boldsymbol{g} = 0$ and

$$\boldsymbol{f} = \begin{pmatrix} \sin(36\pi y)e^{-36\pi^2((x-0.25)^2+(y-0.15)^2+(z-0.25)^2)} \\ 0 \\ 0 \end{pmatrix}. \tag{8.5}$$

Figure 7 compares the wavefields generated by our beam method to those from the FDTD method at $T = 0.2$ along two different lines. As we can see, the Gaussian beam

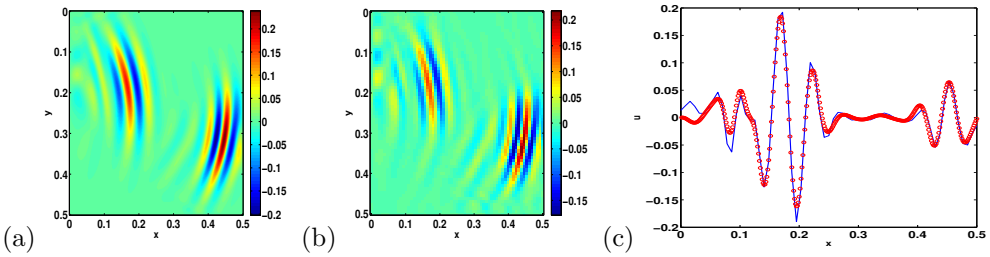

FIG. 6. *Example* 2. *P-wave reflection in a sinusoidal model with Dirichlet boundary conditions.* (a) *FDTD on* $z = 0.25$. (b) *Gaussian beam on* $z = 0.25$. (c) *Comparison on the line* $y = 0.25$ *and* $z = 0.25$*; FDTD: "o"; beam: "-".*

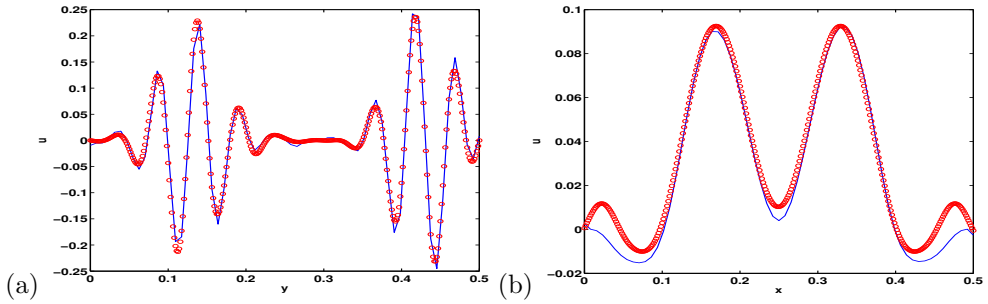

FIG. 7. *Example* 3. *S-wave reflection with a vertical hitting angle.* (a) *On the line* $x = 0.25$ *and* $z = 0.25$ *at* $T = 0.2$. (b) *On the line* $y = \frac{5}{32}$ *and* $z = 0.25$ *at* $T = 0.2$. *FDTD: "o"; beam: "-".*

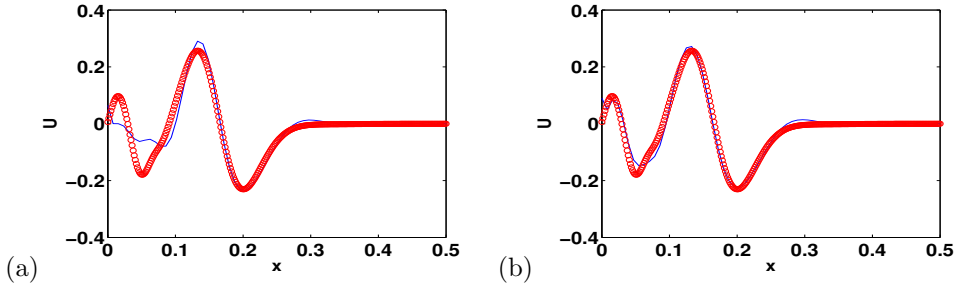

FIG. 8. *Example* 4. *S-wave reflection with an oblique hitting angle.* (a) *Beam solution without reinitialization.* (b) *Beam solution with reinitialization. FDTD: "o"; beam: "-".*

solution matches with the FDTD solution in the large scale, and some asymptotic errors only appear in the place where the wavefield is very weak. In particular, Figure 7 shows that the original method without reinitialization is accurate enough, which is consistent with the illustration in Figure 3: when $\sin(\alpha) = 0$, the regular reflection method is expected to be accurate enough and the above experimental result justifies our conclusion.

8.4.2. Example 4. S-wave reflection with oblique hitting angle. We choose elastic parameters to be $\lambda = 1$ and $\mu = 2$. We take the initial conditions to be $\boldsymbol{g} = 0$ and

$$\boldsymbol{f} = \begin{pmatrix} 2\sin(36\pi y + 18\pi x)e^{-36\pi^2\left((x-0.25)^2+(y-0.15)^2+(z-0.25)^2\right)} \\ -\sin(36\pi y + 18\pi x)e^{-36\pi^2\left((x-0.25)^2+(y-0.15)^2+(z-0.25)^2\right)} \\ 0 \end{pmatrix}. \tag{8.6}$$

We remark that we have chosen the direction of the initial wavepacket so that it will hit the boundary at an oblique angle at a certain time, leading to loss of accuracy for beam reflection dynamics at the boundary.

Figure 8 shows the comparison results, where the comparison is carried out along the x-axis with $z = 0.25$ and $y = 0.125$. Figure 8(a) shows the result without reinitialization. As we can see, although the major part of the waves is captured with good accuracy, the tail region of the Gaussian beam solution is not accurate enough due to the fact that oblique reflection beams induced by the S-to-P wave-mode conversion occur. Figure 8(b) shows the result with reinitialization, where the beam solution with reinitialization shows improved results in the tail region.

The results shown in Figure 8 illustrate that our analysis in section 7 is justified, and the S-to-P beam reflection will lose accuracy to some degree so that it is necessary to incorporate the reinitialization process into the algorithm.

8.4.3. Example 5. S-wave reflection in a linear model. The elastic parameters are chosen to be $\mu = 2 + 0.2y$ and $\lambda = 1$. The initial conditions are taken to be $\boldsymbol{g} = 0$ and $\boldsymbol{f}$ as in (8.6).

Figure 9 compares the wavefields without/with reinitialization to the FDTD result on $z = 0.25$ at $T = 0.14$. As we can see, in the upper left corner of Figure 9(a), there are some significant oscillations in the FDTD result. Without reinitialization, Figure 9(b) shows that the Gaussian beam method is not able to capture those oscillations. With reinitialization, Figure 9(c) shows that the Gaussian beam method is able to capture those oscillations in a much clearer way.

8.4.4. Example 6. S-wave reflection in a sinusoidal model. The elastic parameters are chosen to be $\mu = 2 + 0.2\sin(x)$ and $\lambda = 1$. Since the solution of the S-wave eikonal equation in this sinusoidal model is multivalued in some region, caustics occur in wave propagation. Therefore, it is necessary to use Gaussian beams to treat automatically the resulting high-frequency waves.

Figure 10 compares the Gaussian beam wavefield with reinitialization to the FDTD result on $z = 0.25$ at $T = 0.14$. As we can see, the beam solution matches well with the FDTD solution.

8.5. Dirichlet boundary conditions: Generic initial conditions.

8.5.1. Example 7. General initial conditions and sinusoidal model. We apply our multiscale Gaussian beam method to treat more general initial conditions

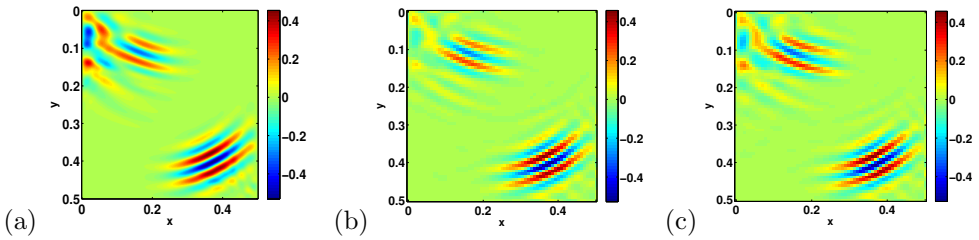

FIG. 9. *Example* 5. *S-wave reflection in a linear model.* (a) *FDTD.* (b) *Beam solution without reinitialization.* (c) *Beam solution with reinitialization.*

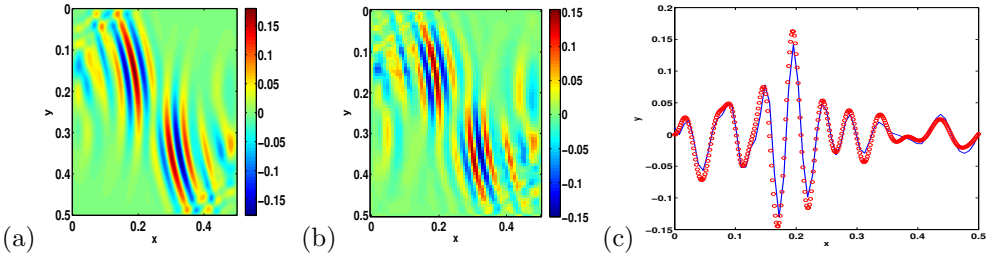

FIG. 10. *Example* 6. *S-wave reflection in a sinusoidal model with reinitialization.* (a) *FDTD.* (b) *Beam solution with reinitialization.* (c) *Comparison on the line* $y = \frac{5}{32}$ *and* $z = 0.25$ *at* $T = 0.14$*; FDTD: "o"; beam: "-".*

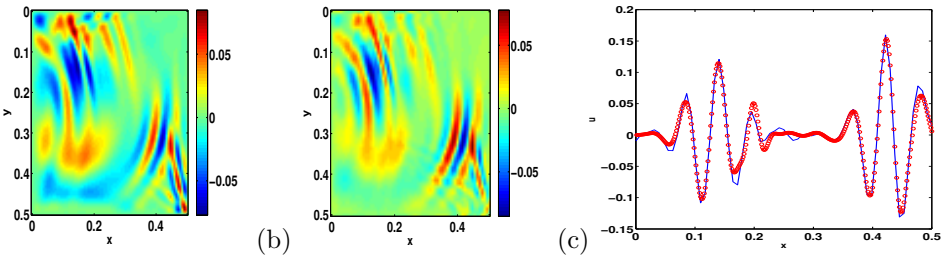

FIG. 11. *Example* 7. *The second component of elastic waves.* (a) *FDTD.* (b) *Beam solution with reinitialization.* (c) *Comparison along a line, where* $y = z = 0.25$*; FDTD: "o"; beam: "-".*

by choosing elastic parameters to be $\lambda = 1+\sin(4\pi x)$ and $\mu = 2$. The initial conditions are taken to be $\boldsymbol{g} = 0$ and

$$\boldsymbol{f} = \begin{pmatrix} \sin(32\pi x + 32\pi y^2)e^{-36\pi^2\left((x-0.15)^2+(y-0.25)^2+(z-0.25)^2\right)} \\ \sin(32\pi x + 10\pi y)e^{-36\pi^2\left((x-0.15)^2+(y-0.25)^2+(z-0.25)^2\right)} \\ \sin(16\pi z)e^{-36\pi^2\left((x-0.15)^2+(y-0.25)^2+(z-0.25)^2\right)} \end{pmatrix}. \tag{8.7}$$

Figure 11 shows comparison results for the second component of the elastic wavefields between FDTD and Gaussian beams on $z = 0.25$ at $T = 0.2$. In this case, P and S waves are captured simultaneously, and wave-mode conversions after reflection are also captured. Figure 11(c) shows that the proposed multiscale Gaussian beam method is able to compute the overall wave motion very well, and slight discrepancies with the FDTD solution occur only at locations where the wavefield is so weak that the asymptotic error dominates.

8.5.2. Convergence rate analysis. Finally, we carry out analysis of the convergence rate. The elastic parameters are taken to be $\lambda = 1$ and $\mu = 2$, and the initial conditions are set to be $\boldsymbol{g} = 0$ and

$$\boldsymbol{f} = \begin{pmatrix} \sin(\eta(16\pi x + 8\pi y))e^{-42\pi^2\left((x-0.25)^2+(y-0.15)^2+(z-0.25)^2\right)} \\ \sin(\eta(16\pi x + 8\pi y))e^{-42\pi^2\left((x-0.25)^2+(y-0.15)^2+(z-0.25)^2\right)} \\ 0 \end{pmatrix}, \tag{8.8}$$

where the amplifying factor η is taken to be a geometric series, $1, 1.5, 2.25, \ldots, 1.5^5$.

Since the convergence rate of an asymptotic method is measured in terms of the inherent small/large parameter, such as the smallest wavelength or the largest frequency parameter, rather than the grid size as used in standard finite element or finite difference methods, we will measure the convergence rate of our multiscale Gaussian beam method in terms of the inherent oscillation frequency, such as $16\pi\eta$ specified by the initial condition (8.8) in the above particular example, where η varies.

Figure 12 shows the results of convergence rate, where the blue star line is the logarithm of the L_2 norm of the error at different η's, and the red line is the linear function with the slope as $-\frac{1}{2}\log(1.5)$. Since the convergence rate of the multiscale Gaussian beam method for acoustic wave equations is $\frac{1}{\sqrt{\omega}}$ as proved in [5], our multiscale Gaussian beam method for elastic wave equations is expected to have a similar convergence rate, such as $O(\frac{1}{\sqrt{\omega}})$, which is evident in the figure. Since a very large η in the above example will induce extremely oscillatory wave phenomena, the FDTD method will demand an extremely fine mesh to resolve these oscillations. Although we

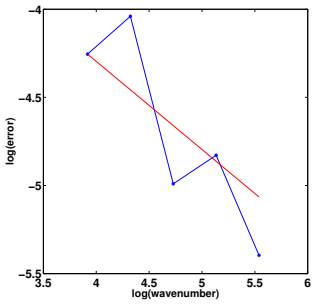

FIG. 12. *Log-log plot for convergence rate of the new Gaussian beam method, where the error curve is "-*" and the line with the slope of* $-\frac{1}{2}\log(1.5)$ *is "-".*

are already using GPUs in our FDTD implementation, the computational resources available to us are still limited. Consequently, we are only able to calibrate the convergence rate of beam solutions in terms of very modest frequencies in terms of η so that the convergence rate as shown in Figure 12 is not so clean.

9. Conclusion. We proposed a new fast multiscale Gaussian beam method to solve the 3-D elastic wave equation in a bounded domain in the high-frequency regime. We have developed a novel multiscale transform to decompose an arbitrary vector-valued function into multiple Gaussian wavepackets with various resolutions. To improve efficiency and accuracy of multiscale beam propagation, we have developed a reinitialization strategy based on the stationary phase approximation method so that we can sharpen each single beam. Numerical examples in different setups demonstrated correctness and robustness of the new method.

Appendix A. Hessian: Positive definite imaginary part. In this appendix, we prove the following theorem.

THEOREM A.1. *Every Gaussian beam preserves the SPD property of the imaginary part of its Hessian after reflection if it is neither grazing nor evanescent after reflection.*

Without loss of generality, we assume that the reflection happens on the surface $\{\boldsymbol{x} = (x, y, z) : \ x = 0\}$. We use τ to denote both P- and S-wave phase functions, and the same applies to the velocity notation c. To simplify the presentation, all Hessian matrices mentioned below refer to the imaginary part only if not specified otherwise. We assume that the reflection point is $\boldsymbol{x}_0 = (x_0, y_0, z_0)$, and all functions are defined at this point if not specified otherwise. We also assume that we treat the positive Hamiltonian throughout this proof, and the negative Hamiltonian will be treated similarly.

A.1. Transformation between Hessian matrices. We first define a new matrix $\tilde{M}$ at the reflection point which takes the following form:

$$\tilde{M} = \begin{pmatrix} \tau_{tt} & \tau_{ty} & \tau_{tz} \\ \tau_{ty} & \tau_{yy} & \tau_{yz} \\ \tau_{tz} & \tau_{yz} & \tau_{zz} \end{pmatrix}. \tag{A.1}$$

Accordingly, we define a transform $\aleph$ between the standard Hessian matrix M (as used before) and $\tilde{M}$ by using the eikonal equation $\tau_t + G(\boldsymbol{x}, \nabla\tau(\boldsymbol{x})) = 0$,

$$\aleph(\tilde{M}) = \begin{bmatrix} \tau_{xx} & \tau_{xy} & \tau_{xz} \\ \tau_{xy} & \tau_{yy} & \tau_{yz} \\ \tau_{xz} & \tau_{yz} & \tau_{zz} \end{bmatrix} \equiv M, \tag{A.2}$$

where all the terms with variables $\boldsymbol{x}$ and t are defined through the eikonal equation as shown in section 5. Moreover, we use $\aleph_P$ and $\aleph_S$ to mean that the transform follows the P-wave eikonal equation and the S-wave eikonal equation, respectively.

If we can prove that the transform $\aleph$ and its inverse transform $\aleph^{-1}$ preserve the SPD property, then Theorem A.1 is proved since $M^{new} = \aleph_P(\tilde{M}) = \aleph_P(\aleph_S^{-1}(M))$ or $M^{new} = \aleph_S(\tilde{M}) = \aleph_S(\aleph_P^{-1}(M))$.

To prove this theorem, instead of considering two types of matrices in (A.2) directly, we will base our proof on the complete $(t, \boldsymbol{x})$-Hessian matrix M_c,

$$M_c = \begin{bmatrix} \tau_{tt} & \nabla\tau_t^T \\ \nabla\tau_t & M \end{bmatrix},$$

where $\nabla\tau_t$ is the gradient of the phase function's time derivative τ_t and M is the standard Hessian. Both $\tilde{M}$ and M are submatrices of M_c.

A.2. Two useful lemmas. To prove the theorem, we need two lemmas. We start with the simpler one, i.e., $\nabla c = 0$ at the point $\boldsymbol{x}_0$.

LEMMA A.1. *If ∇c vanishes at $\boldsymbol{x}_0$, then M_c is a positive semidefinite matrix of rank three.*

Proof. We write out the complete matrix M_c first,

$$\begin{bmatrix} \tau_{tt} & \nabla\tau_t^T \\ \nabla\tau_t & M \end{bmatrix} = \begin{bmatrix} c^2 \frac{\nabla\tau^T}{|\nabla\tau|} M \frac{\nabla\tau}{|\nabla\tau|} & c\frac{\nabla\tau^T M}{|\nabla\tau|} \\ c\frac{M\nabla\tau}{|\nabla\tau|} & M \end{bmatrix}. \tag{A.3}$$

To show that the matrix M_c is positive semidefinite, we let $\boldsymbol{v} = (\alpha, \boldsymbol{p})^T$ and check

$$\boldsymbol{v}^T M_c \boldsymbol{v} = \alpha^2 c^2 \frac{\nabla\tau^T}{|\nabla\tau|} M \frac{\nabla\tau}{|\nabla\tau|} + 2\alpha c \frac{\nabla\tau^T M\boldsymbol{p}}{|\nabla\tau|} + \boldsymbol{p}^T M\boldsymbol{p} \tag{A.4}$$

$$= \left(\alpha c \frac{\nabla\tau}{|\nabla\tau|} + \boldsymbol{p}\right)^T M \left(\alpha c \frac{\nabla\tau}{|\nabla\tau|} + \boldsymbol{p}\right). \tag{A.5}$$

Equation (A.5) shows that the null space of M_c is a 1-D space and its basis can be taken to be $\tilde{\boldsymbol{v}}$, where

$$\bar{\boldsymbol{v}} = \begin{pmatrix} \frac{1}{\sqrt{1+c^2}} \\ -\frac{c}{\sqrt{1+c^2}} \frac{\nabla\tau}{|\nabla\tau|} \end{pmatrix}. \tag{A.6}$$

∎

When $\nabla c \neq 0$ at the point $\boldsymbol{x}_0$, we will follow a similar path as the constant velocity case to show that the imaginary part of the complete matrix M_c is a positive semidefinite matrix.

LEMMA A.2. *The imaginary part of the complete matrix M_c is a positive semidefinite matrix of rank three. Moreover, a single basis element $\bar{\boldsymbol{v}}$ in its null space can be taken to be*

$$\bar{\boldsymbol{v}} = \begin{pmatrix} 1 \\ -c\frac{\nabla\tau}{|\nabla\tau|} \end{pmatrix}. \tag{A.7}$$

Proof. We first prove that $\bar{\boldsymbol{v}}$ is in the null space of

$$\text{Im}(M_c) = \begin{pmatrix} c^2 \frac{\nabla\tau^T \text{Im}(M)\nabla\tau}{|\nabla\tau|^2} & c\frac{\nabla\tau^T \text{Im}(M)}{|\nabla\tau|} \\ c\frac{\text{Im}(M)\nabla\tau}{|\nabla\tau|} & \text{Im}(M) \end{pmatrix}. \tag{A.8}$$

Here, although the gradient of the velocity $\nabla c \neq 0$, this will only affect the real part of M_c. Therefore, we can apply the same argument as in Lemma A.1 to conclude. ∎

Now we are ready to prove the main theorem. The assumption that there are no grazing rays guarantees that $\tau_x \neq 0$ for both beams before and after reflection.

Proof. We start to prove that the transform $\aleph$ and its inverse transform preserve the SPD property when $\nabla c = 0$. In other words, if M is SPD, then $\tilde{M} = \aleph^{-1}(M)$ is SPD. On the other hand, if $\tilde{M}$ is SPD, then $\aleph(\tilde{M})$ is also SPD for both P-wave and S-wave eikonals.

Case 1: $\tilde{M} = \aleph^{-1}(M)$. To prove that $\tilde{M}$ is SPD, we will use two steps: we first consider $\tilde{M}$ to be a submatrix of the corresponding complete matrix M_c, and we then use Lemma A.1 to show that this submatrix is SPD.

For any vector $\tilde{\boldsymbol{u}} = (\tilde{u}_1, \tilde{u}_2, \tilde{u}_3) \in \mathbb{R}^3$, we have

$$\tilde{\boldsymbol{u}}^T \tilde{M} \tilde{\boldsymbol{u}} = \begin{pmatrix} \tilde{u}_1 & 0 & \tilde{u}_2 & \tilde{u}_3 \end{pmatrix} M_c \begin{pmatrix} \tilde{u}_1 \\ 0 \\ \tilde{u}_2 \\ \tilde{u}_3 \end{pmatrix} \tag{A.9}$$

if the reflection happens on the surface $\{\boldsymbol{x} = (x, y, z) : x = 0\}$. Since there is only one single basis element $\bar{\boldsymbol{v}}$ in the null space of matrix M_c as shown in Lemma A.1, all vectors in the form $(u_1, 0, u_2, u_3)^T$ are not parallel to $\bar{\boldsymbol{v}}$. Moreover, since the complete matrix M_c is a positive semidefinite matrix, for any vector $\boldsymbol{u} \in \{\boldsymbol{u} = (\tilde{u}_1, 0, \tilde{u}_2, \tilde{u}_3) : \tilde{\boldsymbol{u}} = (\tilde{u}_1, \tilde{u}_2, \tilde{u}_3)\}$ the right-hand side of (A.9) is positive. Consequently, $\tilde{\boldsymbol{u}}^T \tilde{M} \tilde{\boldsymbol{u}} > 0$ for any $\tilde{\boldsymbol{u}}$ so that $\tilde{M}$ is SPD.

Case 2: $M = \aleph(\tilde{M})$. We will follow the same route as in Case 1. We first treat the Hessian M as a submatrix of the complete matrix M_c and we then use the fact that M_c is a positive semidefinite matrix.

In terms of the transform $M = \aleph(\tilde{M})$, for any vector $\boldsymbol{u} \in \mathbb{R}^3$ we have

$$\boldsymbol{u}^T M \boldsymbol{u} = \begin{pmatrix} 0 & \boldsymbol{u}^T \end{pmatrix} M_c \begin{pmatrix} 0 \\ \boldsymbol{u} \end{pmatrix}. \tag{A.10}$$

Since all the vectors $(0, \boldsymbol{u})^t$ in the above are not in the null space of the complete matrix M_c, where, for any vector $(0, \boldsymbol{u})$, we have

$$(0, \boldsymbol{u})^T \neq \beta \bar{\boldsymbol{v}} \quad \forall \beta \in \mathbb{R}_{\neq 0}, \tag{A.11}$$

we conclude that $\boldsymbol{u}^T M \boldsymbol{u} > 0$ for any $\boldsymbol{u}$ and M is positive definite.

When $\nabla c \neq 0$, we can use the same idea as when $\nabla c = 0$ to prove that the transform $\aleph$ and its inverse transform will preserve the SPD property. The reason is that we only care about the imaginary part of the matrix and the imaginary parts of related matrices are exactly the same as the ones in the constant velocity case. ∎

Acknowledgments. We would like to thank the associate editor and the anonymous reviewers for their constructive comments.

REFERENCES

[1] K. Aki and P. Richards, *Quantitative Seismology*, Freeman and Co., San Francisco, 1980.

[2] V. M. Babich and V. S. Buldyrev, *Asymptotic Methods in Short Wave Diffraction Problems*, Nauka, Moscow, 1972 (in Russian).

[3] I. M. Babuška and S. A. Sauter, *Is the pollution effect of the FEM avoidable for the Helmholtz equation considering high wave numbers?*, SIAM J. Numer. Anal., 34 (1997), pp. 2392–2423.

[4] G. Bao, J. Lai, and J. Qian, *Fast multiscale Gaussian beam methods for wave equations in bounded domains*, J. Comput. Phys., 261 (2014), pp. 36–64.

[5] G. Bao, J. Qian, L. Ying, and H. Zhang, *A convergent multiscale Gaussian-beam parametrix for the wave equation*, Comm. Partial Differential Equations, 38 (2013), pp. 92–134.

[6] A. Bayliss, C. I. Goldstein, and E. Turkel, *On accuracy conditions for the numerical computation of waves*, J. Comput. Phys., 59 (1985), pp. 396–404.

[7] S. Bougacha, J. Akian, and R. Alexandre, *Gaussian beams summation for the wave equation in a convex domain*, Commun. Math. Sci., 7 (2009), pp. 973–1008.

[8] E. Candès and L. Demanet, *The curvelet representation of wave propagators is optimally sparse*, Comm. Pure Appl. Math., 58 (2005), pp. 1472–1528.

[9] E. Candes, L. Demanet, and L. Ying, *Fast computation of Fourier integral operators*, SIAM J. Sci. Comput., 29 (2007), pp. 2464–2493.

[10] E. Candès and D. Donoho, *New tight frames of curvelets and optimal representations of objects with piecewise C^2 singularities*, Comm. Pure Appl. Math., 57 (2004), pp. 219–266.

[11] V. Cerveny, M. Popov, and I. Psencik, *Computation of wave fields in inhomogeneous media-Gaussian beam approach*, Geophys. J. R. Astr. Soc., 70 (1982), pp. 109–128.

[12] L. Demanet and L. Ying, *Wave atoms and sparsity of oscillatory patterns*, Appl. Comput. Harmon. Anal., 23 (2007), pp. 368–387.

[13] L. Demanet and L. Ying, *Wave atoms and time upscaling of wave equations*, Numer. Math., 113 (2009), pp. 1–71.

[14] N. Hill, *Prestack Gaussian-beam depth migration*, Geophysics, 66 (2001), pp. 1240–1250.

[15] L. Hörmander, *On the existence and the regularity of solutions of linear pseudo-differential equations*, Enseign. Math., 17 (1971), pp. 99–163.

[16] L. Hörmander, *The Analysis of Linear Partial Differential Operators*, Vol. 1, 2nd ed., Springer, New York, 1990.

[17] F. Karal, Jr., and J. B. Keller, *Elastic wave propagation in homogeneous and inhomogeneous media*, J. Acoust. Soc. Am., 31 (1959), pp. 694–705.

[18] S. Leung and J. Qian, *Eulerian Gaussian beam methods for Schrödinger equations in the semi-classical regime*, J. Comput. Phys., 228 (2009), pp. 2951–2977.

[19] S. Leung and J. Qian, *The backward phase flow and FBI-transform-based Eulerian Gaussian beams for the Schrödinger equation*, J. Comput. Phys., 229 (2010), pp. 8888–8917.

[20] S. Leung, J. Qian, and R. Burridge, *Eulerian Gaussian beams for high frequency wave propagation*, Geophysics, 72 (2007), pp. SM61–SM76.

[21] A. Martinez, *An Introduction to Semiclassical and Microlocal Analysis*, Springer, New York, 2002.

[22] V. P. Maslov, *The Complex WKB Method for Nonlinear Equations* I*: Linear Theory*, Birkhauser Verlag, Basel, 1994.

[23] J. Qian and L. Ying, *Fast Gaussian wavepacket transforms and Gaussian beams for the Schrödinger equation*, J. Comput. Phys., 229 (2010), pp. 7848–7873.

[24] J. Qian and L. Ying, *Fast multiscale Gaussian wavepacket transforms and multiscale Gaussian beams for the wave equation*, SIAM J. Multiscale Model. Simul., 8 (2010), pp. 1803–1837.

[25] J. Ralston, *Gaussian beams and the propagation of singularities*, in Studies in Partial Differential Equations, AMS/MAA Stud. Math. 23, W. Littman, ed., AMS, Providence, RI, 1983, pp. 206–248.

[26] H. Smith, *A parametrix construction for wave equations with $C^{1,1}$ coefficients*, Ann. Inst. Fourier Grenoble, 48 (1998), pp. 797–835.

[27] A. Taflove and S. C. Hagness, *Computational Electrodynamics: The Finite Difference Time Domain Method*, 2nd ed., Artech House, Norwood, MA, 2000.

[28] N. Tanushev, J. Qian, and J. Ralston, *Mountain waves and Gaussian beams*, SIAM J. Multiscale Model. Simul., 6 (2007), pp. 688–709.

[29] B. S. White, *The stochastic caustic*, SIAM J. Appl. Math., 44 (1984), pp. 127–149.